Semiconductor Package Failure Analysis with ZEISS 3D X-ray Microscopy and LaserFIB

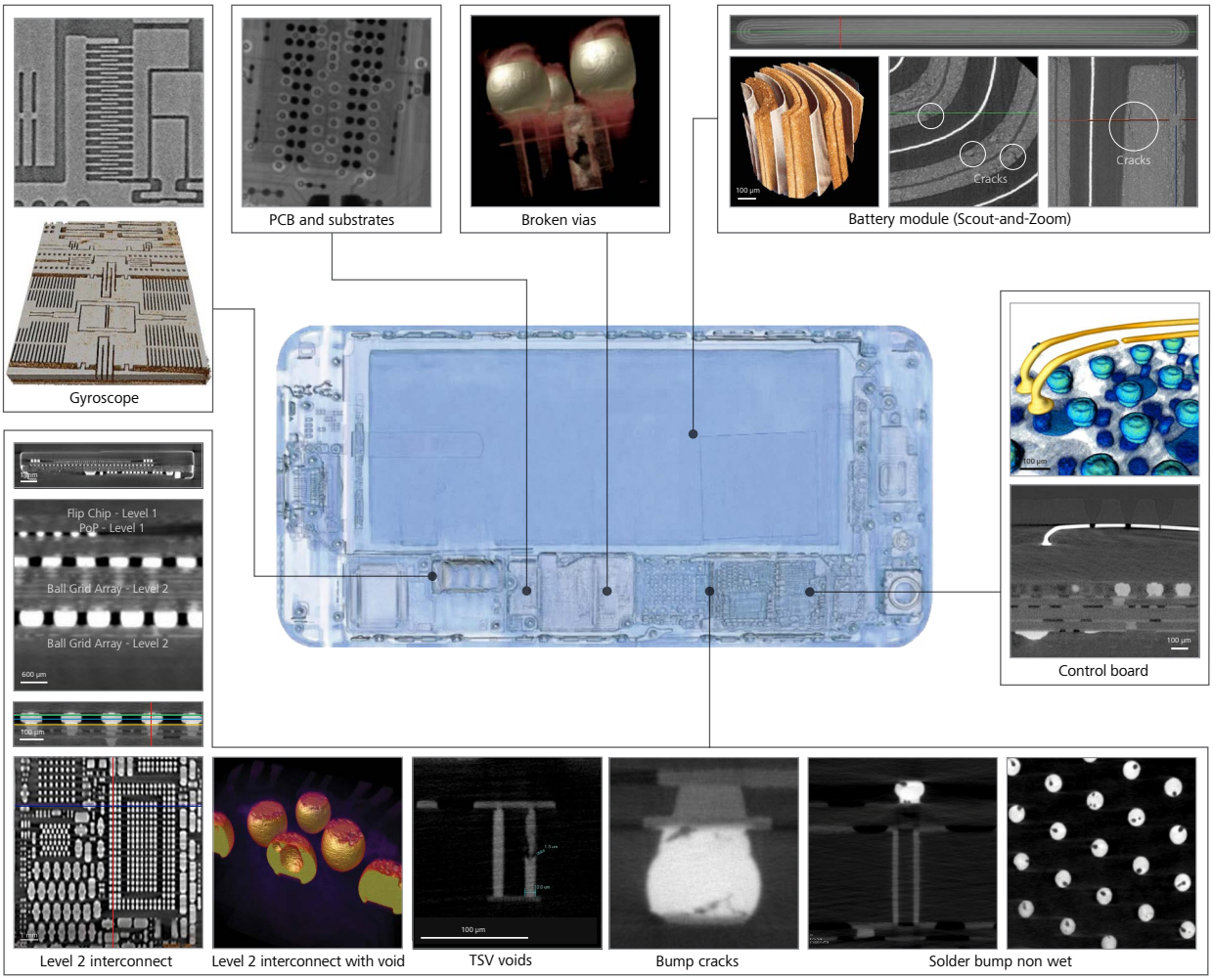

Seeing beyond

Introduction

Seeing beyond

Semiconductor packaging technology advancements are enabling improved system performance beyond transistor scaling. However, increasing density and shrinking of interconnects and complex package architectures introduce new challenges for fault isolation, non-destructive imaging, and physical failure analysis workflows. Advances in 3D X-ray microscopy and AI-enabled reconstruction break traditional barriers of throughput, image quality, field of view and resolution. However, these techniques still face challenges in advanced packages where interconnect pitch and size are in micron scale or below and rely on physical failure analysis (PFA).

X-ray microscopy is still relevant in guiding the sample preparation in PFA, such as determining the region of interest and orientation of the cross-section. In addition, the integration of short-pulsed lasers with FIB-SEMs introduces a new paradigm for high throughput, artifact-free sample preparation of semiconductor packages compared to traditional mechanical methods providing access to deeply buried interconnects and subsequent cross-sectional analysis.

ZEISS has developed a novel correlative workflow connecting these two microscopy techniques where 3D XRM guides precise and targeted sample preparation with fs-laser integrated Ga FIB-SEM, reducing sample preparation and analysis from days to hours. This compendium includes recent publications highlighting this workflow and several use cases that enable sample preparation for fault isolation and physical failure analysis.

Table of Contents

Originally Published at ISTFA 2023: Proceedings from the 49th International Symposium for Testing and Failure Analysis Conference

ZEISS

Seeing beyond

An Artificial Intelligence Powered Resolution Recovery Technique and Workflow to Accelerate Package Level Failure Analysis with 3D X-ray Microscopy

Syahirah Mohammad-Zulkifli, Bernice Zee, Qiu Wen, Maverique Ong
Advanced Micro Devices (Singapore) Pte Ltd, Device Analysis Lab

Yanjing Yang, Andriy Andreyev, Masako Terada, Allen Gu
Carl Zeiss Microscopy

Abstract

3D X-ray microscopy (XRM) is an effective high-resolution and non-destructive tool for semiconductor package level failure analysis [1-3]. One limitation with XRM is the ability to achieve high-resolution 3D images over large fields of view (FOVs) within acceptable scan times. As modern semiconductor packages become more complex, there are increasing demands for 3D X-ray instruments to image encapsulated structures and failures with high productivity and efficiency. With the challenge to precisely localize fault regions, it may require high-resolution imaging with a FOV of tens of millimeters. This may take over hundreds of hours of scans if many high-resolution but small-volume scans are performed and followed with the conventional 3D registration and stitches. In this work, a novel deep learning reconstruction method and workflow to address the issue of achieving high-resolution imaging over a large FOV is reported. The AI powered technique and workflow can be used to restore the resolution over the large FOV scan with only one high-resolution and one large FOV scan. Additionally, the 3D registration and stitch workflow are automated to achieve large FOV images with a recovered resolution comparable to the actual high-resolution scan.

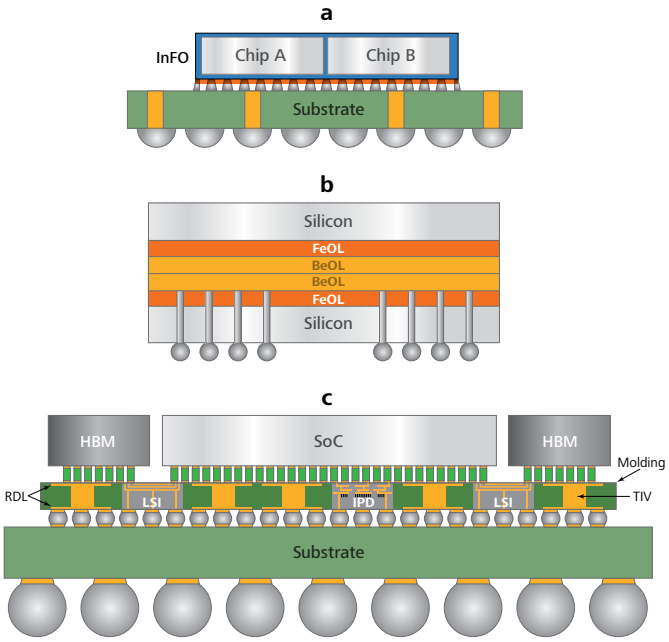

Figure 1 *Illustration examples of next generation packaging technologies used for heterogenous integration; a) WLFO, b) TSV, and c) embedded bridges [4].*

Introduction

The pace of adopting next generation packaging technologies for heterogeneous integration has picked up significantly as the cost of transistor scaling has risen astronomically. Examples of such packaging technologies include Wafer-Level Fan-Out (WLFO), Through-Silicon-Vias (TSV), 3D interconnects and embedded bridges as shown in Figure 1.

Next generation packaging technologies present interesting challenges to current failure analysis techniques. The ability to localize and visualize defects prior to and during physical failure analysis (PFA) is no longer straightforward. Complex die stacking and numerous die-to-die interconnects with no direct electrical contact make package-level electrical fault isolation (EFI) difficult.

The resolution of non-destructive imaging techniques has also been pushed to theoretical limits in imaging highly miniaturized interconnects. Consequently, 3D X-ray microscopy (XRM) has become the preferred non-destructive imaging tool for semiconductor package failure analysis because of its high-resolution imaging capabilities [1-3]. It has become a critical tool because of its ability to clearly image different interfaces of complex multichip packages. However, trade-offs in terms of FOV, image signal-to-noise ratio (SNR), and scan times must be balanced. To overcome these constraints, machine learning methodologies are being applied to the reconstruction step to enhance imaging efficiency and quality.

A deep learning based high-resolution reconstruction method capable of speeding up data acquisition by at least a factor of four without the need of beamline hardware in the 3D XRM tool was recently reported [5-6]. Improved scan throughput was achieved through the implementation of pre-trained neural networks which extract signals from low-dose data more efficiently than the conventional Feldkamp-Davis-Kress (FDK) method. However, this methodology can only be applied to small FOV, high-resolution scans. As larger multichip packages with complex routing and stacking becomes more mainstream, there is a growing need for large FOV, high-resolution imaging.

In this paper, another novel deep learning-based reconstruction method capable of learning the point spread function (PSF) of low-resolution data in a neural network training process is described. Through this new methodology, the resolution of low-resolution data with a large FOV is restored through an inference process without physically performing numerous high-resolution scans. We will demonstrate on several IC packages that the proposed workflow can be utilized in imaging circuit interconnect elements in a large area, in which standard XRM has not been practically possible due to the trade-off of image resolution and FOV.

DeepScout Methodology

DeepScout is a novel image reconstruction method that tackles the problem of large FOV, high-resolution imaging by using a deep-learning algorithm to learn the effective point spread function (PSF) of the imaging device and then use it to perform deconvolution and improve the spatial resolution.

In the first stage of the DeepScout workflow, two datasets need to be acquired on the same object at low-resolution and high-resolution. The acquisition parameters for low-resolution and high-resolution datasets are chosen in such a way that the voxel size ratio is less than six, where the high-resolution volume is contained inside the low-resolution volume and is representative of the object interiors. Then the two datasets are reconstructed and registered to ensure precise correspondence between the same features imaged at low and high resolution. Such a registered image pair is then passed to the DeepScout neural network for training, where the network will learn to create a mapping from low resolution to high resolution. A complete description of the DeepScout training process and network is out of the scope of this paper. For further details please refer to Ref. [7]. After the training is complete, the trained DeepScout model can then be used to improve the spatial resolution of the entire low-resolution dataset, or another dataset acquired in similar conditions for the same or equivalent sample type.

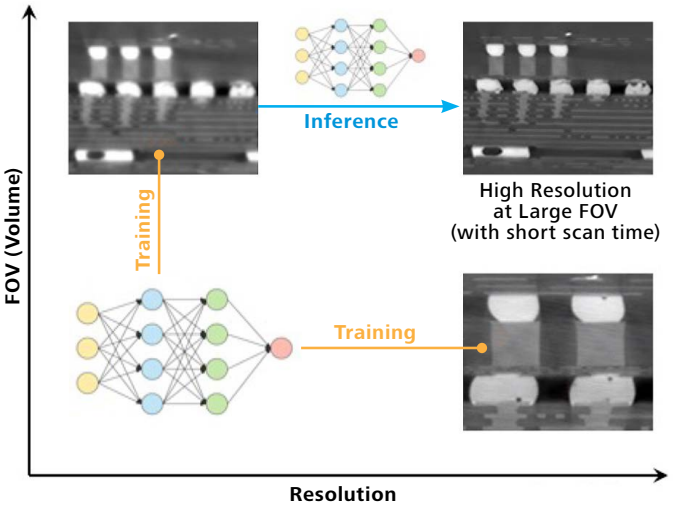

Figure 2 *The schematics of the DeepScout reconstruction method to restore image resolution from the low-resolution image input.*

This procedure is summarized in Figure 2. DeepScout can mitigate the trade-off between slow acquisition and high resolution by learning thedependencies between low-resolution and high-resolution datasets.

Case Studies

Case Study 1: Embedded Bridge Package

An advanced stacked die package with interconnectivity issues was sent in for failure analysis (FA). As per traditional FA flow, a non-destructive C-Mode Scanning Acoustic Microscopy (CSAM) test was performed to isolate the fault. CSAM results showed an anomaly spanning across the majority of the length of the unit in Figure 3. To understand the nature and location of the failure, a DeepScout scan to image the internal structures was done. This scan was able to capture a large FOV at the anomaly region with a high resolution of 0.72 µm/voxel.

From the 3D XRM DeepScout scan results, notch-like defects were clearly resolved across the row of microbumps. A comparison at the same FOV between the 0.4X objective scan in Figure 4a and the DeepScout scan in Figure 4b shows better resolved features for the reconstructed image obtained with DeepScout. Figure 4c is the actual high-resolution scan at 0.72 µm/voxel resolution used for training the network model in DeepScout method.

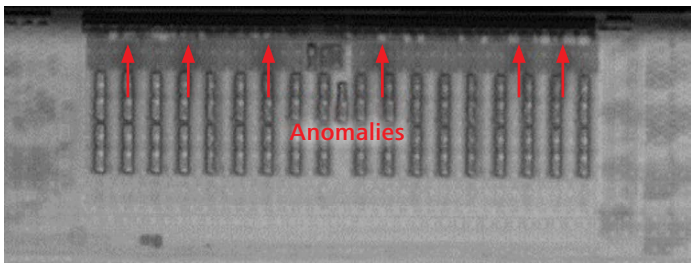

Figure 3 *CSAM image showing anomalies at the microbump interface.*

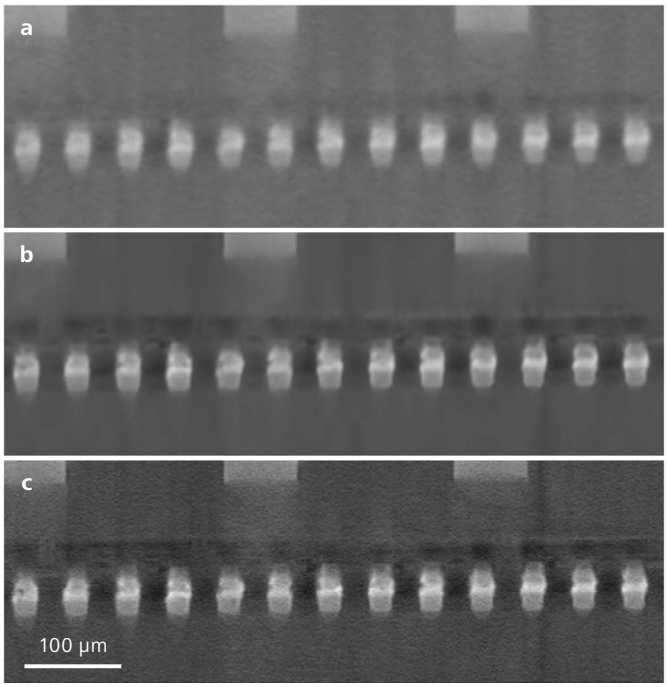

Figure 4 *Reconstructed microbump image with notches a) a virtual cross-section of a low-resolution scan at 2.3 µm/vox resolution; b) a virtual slice of the DeepScout volume; and c) the high-resolution scan data at 0.72 µm/vox resolution used for training the network model in DeepScout method.*

Case Study 2: WLFO Package

Ultra-short reach (USR) bump fails were reported for a WLFO unit in this case study. As there are no ball out for these USR bumps, fault isolation through electrical techniques is not possible. To assist in the fault isolation, 3D XRM was used to give an overview of the internal layers and check if any defects could be observed. The 3D XRM scan requires a large FOV to target the failing USR bumps and corresponding redistribution layer (RDL) traces between graphics core die (GCD) and memory-controlled die (MCD). High-resolution scans are also required to visualize the fine bump pitch and line width spacing at the RDL and USR layers. To ensure both requirements are fulfilled, a DeepScout scan was performed.

At the same FOV, the reconstructed image obtained with DeepScout on Figure 5b shows better resolved RDL traces and USR bumps compared to Figure 5a, which was obtained using the 0.4X objective. The example demonstrates the resolution on small structures can be restored with the DeepScout method and workflow. More importantly, the volume of DeepScout is the same as the large FOV scan at 2.1 µm/voxel.

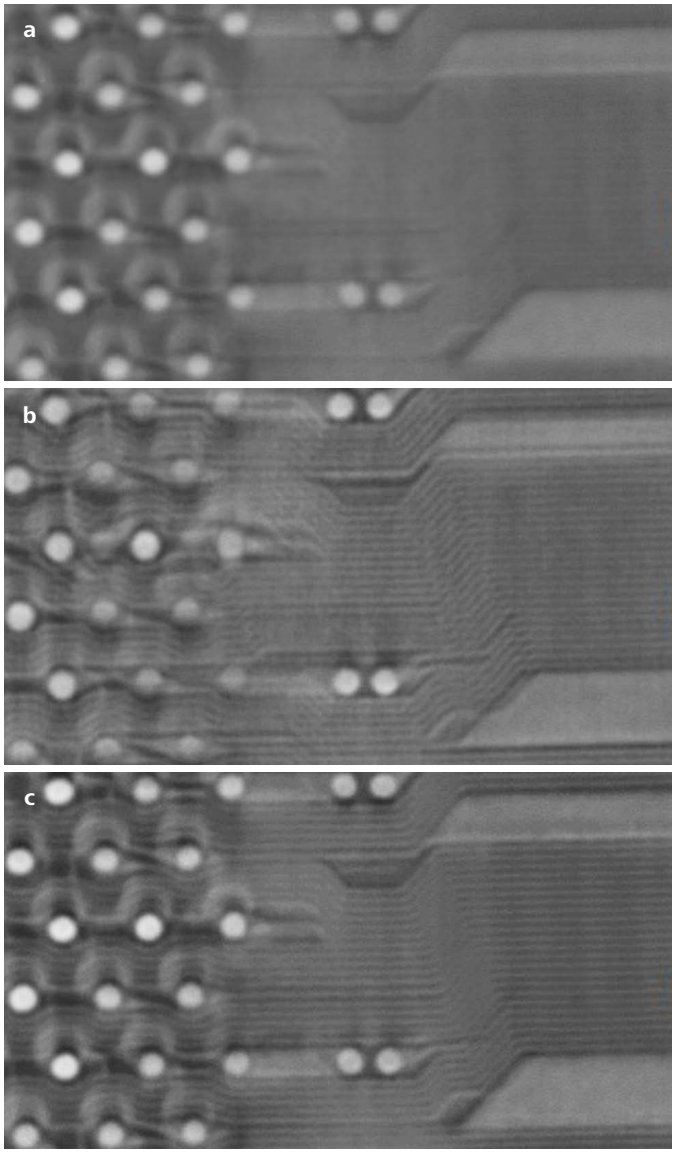

Figure 5 *A DeepScout example. a) a virtual planar view of a low-resolution scan at 2.1 µm/vox resolution; b) a virtual slice of the DeepScout volume; and c) the high-resolution scan data at 0.7 µm/vox resolution used for training the network model in DeepScout method.*

Although there were no obvious anomalies from the 3D XRM images, the data from these scans has provided the analyst with a guide of the overview across a large FOV of the different layers as shown in Figure 6. Because of the enhanced resolution on a DeepScout volume, it provides guidance and assurance for the analyst on how to proceed in the subsequent PFA to ensure successful root cause analyses. In this case we focused on the USR MCD interconnect during PFA based on the DeepScout data and a via crack defect was captured and visualized with a FIB-SEM workflow per Figure 7.

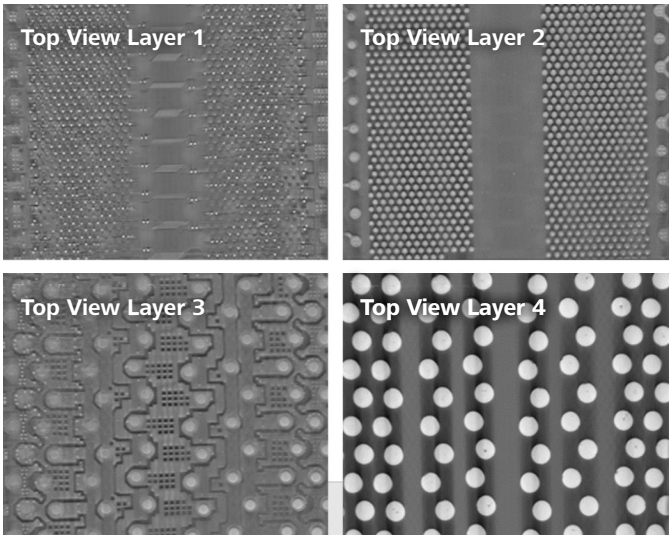

Figure 6 *3D XRM DeepScout virtual planar slice view of multiple layers of the WLFO package over a large FOV.*

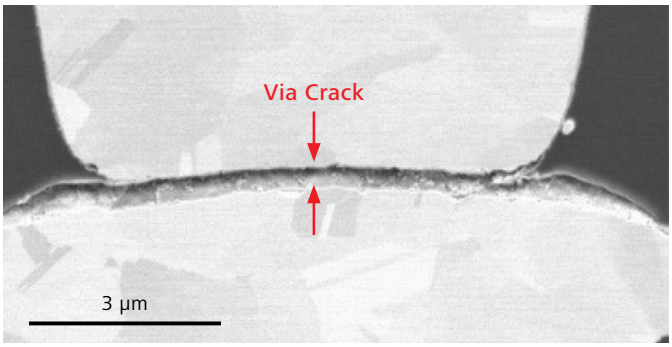

Figure 7 *Image of USR MCD interconnect showing via crack observed after PFA using focused ion beam (FIB).*

Case Study 3: Embedded Bridge Package

In this case study, an embedded bridged advanced stacked die package was reported as failing power supply short. Curve trace verification and CSAM imaging revealed an anomaly in one segment of the package. From the CSAM image shown in Figure 8, it was not apparent if the observed anomaly was confined to the microbump interface or if it has extended to the C4 bump interface.

Hence, 3D XRM was carried out at the region of interest to verify the anomaly and determine the cause of short failure. Due to the extent of the damage observed via CSAM, imaging a large FOV with high resolution was required. From Figure 9, for the same FOV, the reconstructed image obtained with DeepScout on the bottom using the 4X objective shows better resolved microbumps than the image on the top which was obtained using the 0.4X objective. DeepScout allows FA engineers to acquire 3D X-ray data with both large FOV and high-resolution benefits.

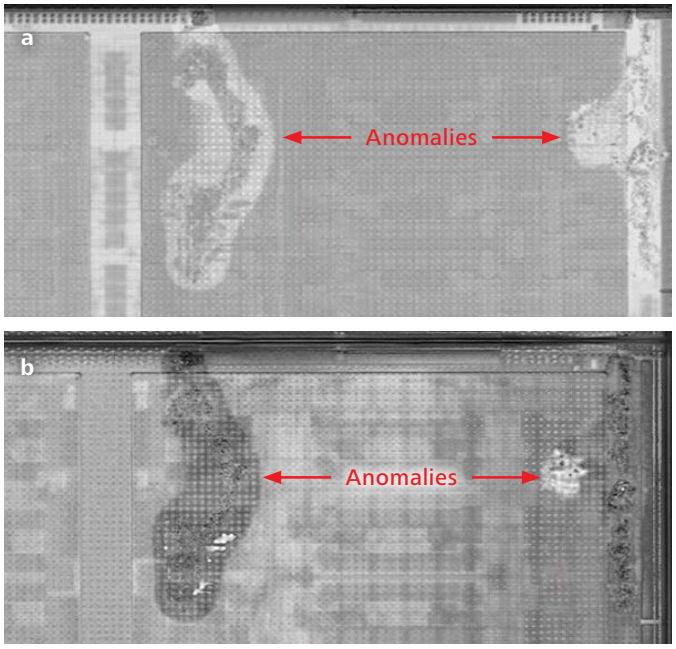

Figure 8 *CSAM image showing anomaly at the a) microbump interface and b) C4 bump interface.*

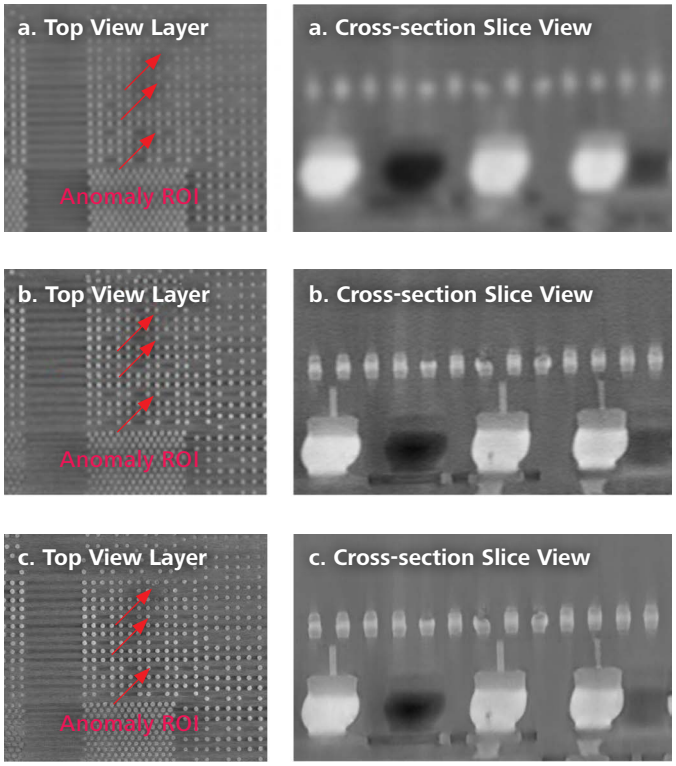

Figure 9 *A virtual planar and cross-section slice obtained from a) 0.4X objective at 7.82 µm/vox resolution reconstructed with conventional FDK method; b) 4X objective at 1.4 µm/vox resolution reconstructed with conventional FDK method; and c) 4X objective at 1.4 µm/vox resolution reconstructed with DeepScout method that was trained with high-resolution scan data at 0.7 µm/vox resolution.*

Conclusion

3D XRM has become the preferred non-destructive imaging tool for semiconductor package failure analysis because of its high-resolution imaging capabilities. However, as new package architectures trend towards 3D stacking and multichip modules, interconnect densification and miniaturization as well as increased package size presents a challenge in structural and failure analysis, because the tradeoff between resolution and FOV is one of the fundamental limitations in microscopy and microanalysis [7]. In this paper, deep learning powered X-ray imaging technique DeepScout has shown the capability to address the issue of achieving high resolution at a large area. We have shown several case studies of complex advanced packages with the technique.

Acknowledgment

The authors would like to thank their colleagues who have contributed to this work.

References

[1] L. Mirkarimi, A. Gu, L. Hunter, G. Guevara, M. Huynh, R. Katkar, "X-ray Microscopy and Root Cause Analysis in Electronic Packaging", *Proc 41st Int'l Symp for Testing and Failure Analysis,* Portland, OR, Nov. 2015, pp. 430-435. doi: 10.31399/asm.cp.istfa2015p0430

[2] A. Gu, J. Auyoong, "3D Measurement Workflow for Packaging Development and Production Control Using High-Resolution 3D X-ray Microscope", *2018 IEEE 20th Electronics Packaging Tech Confer (EPTC),* Singapore, Dec. 2018. doi:10.1109/EPTC.2018.8654390

[3] S. M. Zulkifli, B. Zee, W. Qiu, A. Gu, "High-Res 3D X-ray Microscopy for Non-Destructive Failure Analysis of Chip-to-Chip Micro-bump Interconnects in Stacked Die Packages", *IEEE 24th Int'l Symp on the Physical and Failure Analysis of Integrated Circuits (IPFA),* Chengdu, China, Jul. 2017. doi:10.1109/IPFA.2017.8060111

[4] 3DFabric | TSMC. (n.d.). Retrieved April 11, 2023, from https://3dfabric.tsmc.com/english/dedicatedFoundry/technology/3DFabric.htm

[5] A. Gu, A. Andreyev, M. Terada, B. Zee, S. M. Zulkifli, Y. Yang, "Accelerate Your 3D X-ray Failure Analysis by Deep Learning High Resolution Reconstruction Paper," Int'l Symp for Testing and Failure Analysis, No: istfa2021p0291, pp. 291-295, Phoenix, AZ, Dec 2021.

[6] A. Gu, M. Terada, H. Stegmann, T. Rodgers, C. Fu and Y. Yang, "From System to Package to Interconnect: An Artificial Intelligence Powered 3D X-ray Imaging Solution for Semiconductor Package Structural Analysis and Correlative Microscopic Failure Analysis," IPFA 2022, Singapore.

[7] M. Andrew, A. Andreyev, F. Yang, M. Terada, A. Gu, R. White, "Fully automated deep learning based resolution recovery", SPIE Advances in X-ray Imaging, 2022. https://doi.org/10.1117/12.2633095.Z

Originally Published at ISTFA 2023: Proceedings from the 49th International Symposium for Testing and Failure Analysis Conference

ZEISS

Seeing beyond

Detecting Wafer Level Cu Pillar Defects Using Advanced 3D X-ray Microscopy (XRM) with Submicron Resolution

Susan Li, John Frame, Edita Madriaga-Berry, Jose Hulog, Ming Zhang
Infineon Technology

Masako Terada, Allen Gu, David Taraci
Carl Zeiss Microscopy

Abstract

In this work we present a new defect localization capability on Wafer Level Chip Scale Packages (WLCSP) with small-scale Cu pillars using advanced 3D X-ray microscopy (XRM). In comparison to conventional microcomputed tomography (Micro-CT or microCT) flat-panel technology, the synchrotron-based optically enhanced 3D X-ray microscopy can detect very small defects with submicron resolutions. Two case studies on actual failures (one from the assembly process and one from reliability testing) will be discussed to demonstrate this powerful defect localization technique. Using the tool has helped speed up the failure analysis (FA) process by locating the defects non-destructively in a matter of hours instead of days or weeks as needed with destructive physical failure analysis.

Introduction

2D X-ray imaging and inspection remain the most commonly used X-ray technique. Incident X-ray irradiates samples and a 2D detector is utilized to collect shadow or projection images, where absorption contrast is generated by the difference in X-ray absorption between different materials or thickness. This technique, however, is not adequate for revealing true 3D structures because it projects 3D objects to a 2D plane. As a result, when it is used for semiconductor packages, important information such as internal faulty regions of a device may remain hidden due to complicated multi-layer structures. The disadvantage may be overcome by using 3D X-ray computed tomography (CT) technique.

In a CT system, a series of 2D projection views is captured at different angles while the specimen rotates. These 2D images are used to reconstruct 3D X-ray tomographic volume by applying mathematic models and algorithms. The spatial resolution of the imaging technique can be improved by the integration of an optical microscopy system. The improved technology, named as 3D X-ray microscopy (XRM), was used in this work for highresolution 3D imaging, providing an insightful vision for non-destructive FA technology.

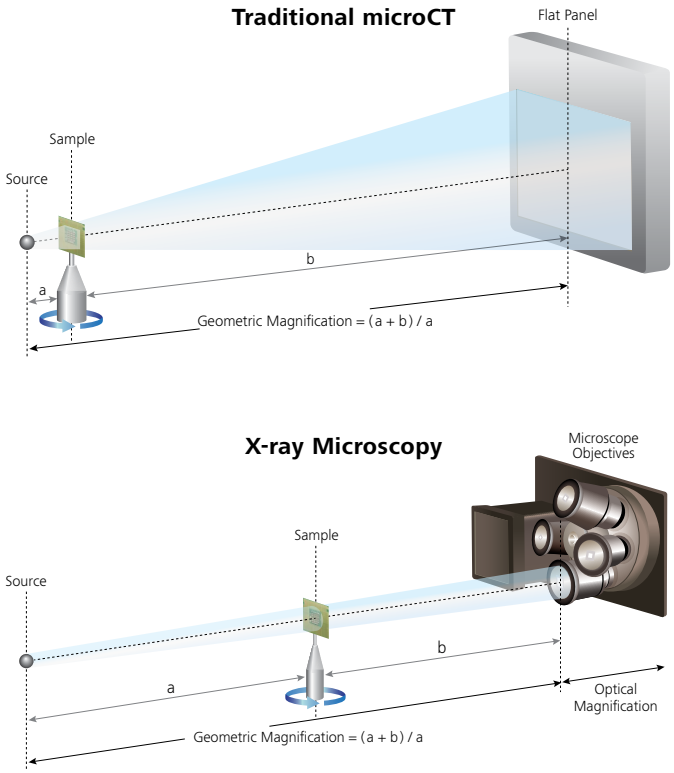

Figure 1 *Comparison of XRM optical architecture with traditional microCT.*

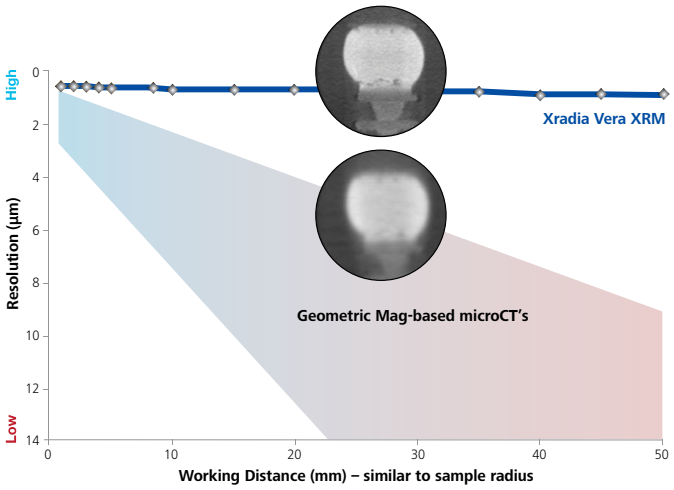

Figure 2 *Resolution performance comparison between traditional microCT and XRM. The sample was about 55x55 mm in size.*

Figure 1 shows the comparison of the setup of a 3D XRM with the traditional microCT. In the XRM configuration, a high-resolution X-ray scintillator is coupled with optical lens system to further magnify the image and improve spatial resolution and contrast. This architecture with two-stage magnification mechanism is unique to provide the necessary resolution required to image subtle internal defects of large electronic devices (Figure 2). Because XRM's unique resolution-at-a-distance capability, XRM can be used to detect many different types of failure modes, shown in Figure 3.

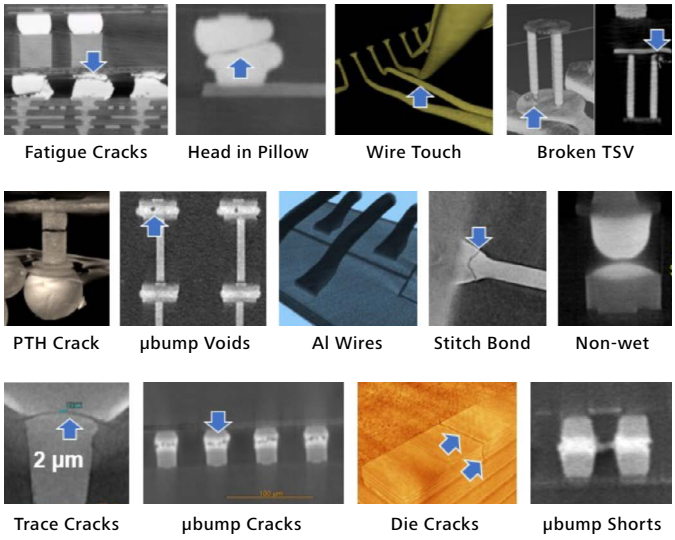

Figure 3 *A variety of defect types that can be detected with 3D X-ray microscopy with the sample sizes ranging from a few mm to tens of mm.*

3D X-ray tools have been widely used for non-destructive failure analysis to inspect wire-bonding related defects, solder joints and die attach voids, and other anomalies on printed circuit boards (PCBs) and IC packages [1]. 3D CT scanning compiles digital X-ray images into a 3D volume, resolving internal structures that can be virtually sliced, measured and viewed at any angle digitally, all without physically damaging actual parts [2-5]. A conventional flat-panel Micro-CT X-ray system can achieve resolutions of the order of 2-10 µm depending on the size and materials of a device being analyzed and can reveal defects such as fused bond wires or wires touching the lead post [6] (Figure 4).

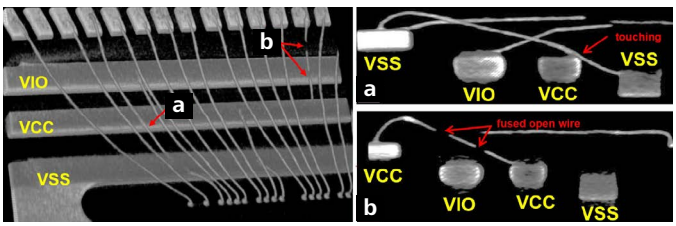

Figure 4 *Conventional Micro-CT images showed a bond wire touching the lead post (a) and a fused open bond wire (b).*

However, it normally cannot detect small, subtle defects such as separated solder joint interfaces, slightly lifted wire bonds, or bump cracks. It also cannot reveal the details on small-scale Cu pillars (25-30 µm in diameter), such as those used by an automotive fingerprint sensor (Figure 5a).

Advanced 3D XRM systems utilize the innovations first developed for synchrotron-based instruments. It uniquely employs scintillator-coupled optics as an integral part of the X-ray detector. Unlike conventional Micro-CT techniques, where spatial resolution solely relies on geometric magnification, the optical objective-based XRM utilizes a unique two-stage magnification mechanism to achieve high resolution over large working distances. Better resolution can be achieved even for large semiconductor package samples. The latest 3D XRM system enables users to visualize and quantify internal structures with resolution down to 0.45 µm, significantly beyond the conventional Micro-CT flat-panel technology.

This advanced XRM tool is ideal for revealing defects in the fingerprint sensor's small-scale Cu pillars – defects which other conventional Micro-CT X-ray systems cannot detect. Without any sample preparation, the data of a targeted area was acquired at 0.72 µm/voxel resolution with 70 kV X-ray source energy and a 4X objective in XRM. It took about 1.3 hours for the 3D scan and reconstruction, and the detailed small-scale Cu pillars' joint conditions including solder joint non-wetting and cracking were revealed (Figures 5b, 5c and 5d).

In this paper, we will describe how to use the latest 3D XRM tool to analyze failing devices from the assembly process and after reliability testing and obtain very impressive results in a much shorter analysis cycle time.

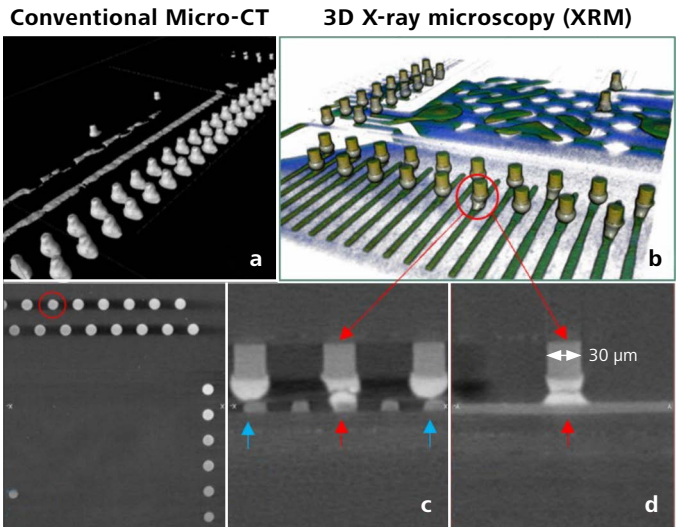

Figure 5 *Compared to a) conventional Micro-CT X-ray, b) 3D XRM reveals more details of the small-scale Cu pillars including solder joint non-wetting (blue arrows) and cracking (red arrows) (c and d).*

Results and Discussion

The failing device analyzed is a fingerprint sensor with a Flip-Chip die mounted on a PCB substrate through small-scale Cu pillars. It is used for automotive applications and is therefore subjected to stringent reliability tests. Some failures were observed after 1000 cycles of temperature cycling test, while others were found right after the assembly process. Two units with failures at transmit (TX) or receive (RX) pins were selected for the 3D XRM analysis.

Case Study 1

One fingerprint sensor device failed at three RX pins and three TX pins right after assembly process. 2D X-ray inspection was initially performed on the unit, and an abnormally shaped Cu pillar was found at one of the failing RX pins, but nothing abnormal could be seen at other failing RX and TX pins.

The intact unit was then analyzed using 3D XRM at the failing RX and TX pins. The scan was performed at 0.73 µm/voxel resolution at 70 kV for 1.3 hours. The detailed 3D X-ray images showed the deformed Cu pillar with a shorter Cu stem, open solder joint, and even a slightly bent Cu trace at the affected failing RX pin where an anomalous Cu pillar was detected under the 2D X-ray inspection (Figure 6). The 3D X-ray analysis also showed non-wetting solder joints at the other failing RX and TX pins that conventional Micro-CT could not see (Figure 7).

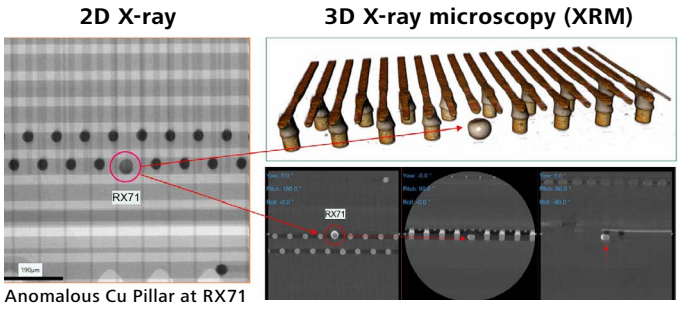

Figure 6 *3D X-ray microscope image can resolve the detailed structure and defects at the deformed Cu pillar of the failing RX pin.*

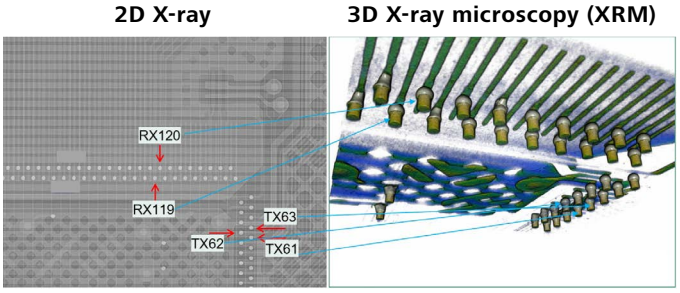

Figure 7 *The detailed 3D X-ray images revealed non-wetting solder caps at all reported failing RX and TX pins, indicated by original round solder caps (the rest of non-wetting pins shown were not electrically tested).*

The scan was performed with 1 µm/voxel resolution and completed within 1 hour. These findings enabled us to visualize the defects in detail, and the information was quickly fed back to the assembly team to implement corrective actions.

Case Study 2

Another fingerprint sensor device showed a partial panel failure at one single RX pin after 1000 temperature cycles. Optical and Scanning Electron Microscope (SEM) inspection revealed an anomaly, possibly package surface damage, at the physical location where the partial panel failure was detected through the electrical testing (Figure 8).

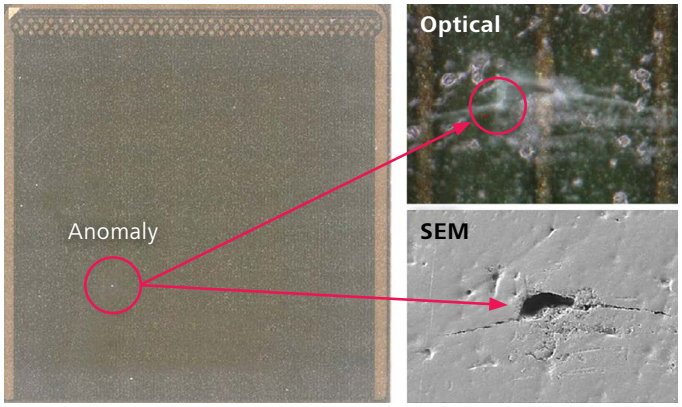

Figure 8 *Optical and SEM inspection showed an anomaly at the reported partial panel failing location.*

The unit was then analyzed using 3D XRM with focus on the anomalous location. The detailed 3D X-ray image showed a cut open Cu trace underneath the anomaly (Figure 9).

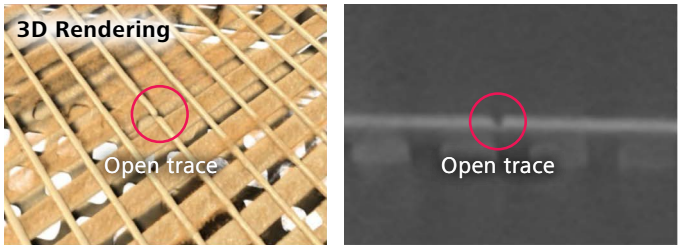

Figure 9 *3D X-ray image showed cut open Cu trace at the anomalous location where the partial panel failure was detected.*

To further understand the failure mechanism, FIB cross-section was performed at the affected location, and the result showed a sharp-edged SiO_2 piece pressed through the package surface, cutting the Cu trace (Figure 10). After checking the socket for ATE testing, it was confirmed that the affected location was right underneath the clamp of the test socket.

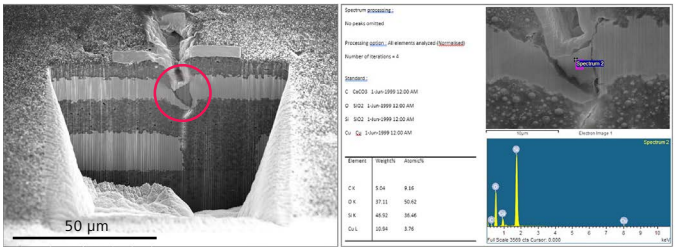

Figure 10 *FIB cross-section at the anomalous location showed a sharp-edged particle pressed into the package, cutting open the Cu trace underneath. EDX analysis showed the particle to be a piece of* SiO_2.

It is presumed that a loose particle landing on the package surface was pressed into the package surface during clamping of the test socket, cutting the Cu trace underneath. The damaged Cu trace became completely open after 1000 temperature cycles. The information was then provided to the product team for improving ATE test conditions and test socket cleanliness.

Conclusions

The analysis results obtained from this advanced 3D X-ray microscope tool significantly exceeded our expectations from a typical Micro-CT X-ray tool, and sped up the FA process by finding defects non-destructively in a matter of hours instead of days or weeks as would be the case with destructive physical failure analysis.

Acknowledgements

The authors would like to thank Robert Blazer from Infineon San Jose FA lab and Claudia Keller from Infineon Munich FA lab, for their helpful review of this paper.

References

[1] Tom Moore; Cheryl Hartfield, "X-ray and SAM – Challenges for IC Package Inspection," *ISTFA 2022,* Pasadena, California

[2] Cheryl Hartfield, "Nanoscale 3D X-ray Microscopy for High Density Multi-Chip Package FA," *ISTFA 2018,* Phoenix, Arizona

[3] S. M. Zulkifli, B. Zee, W. Qiu, A. Gu, "High-Res 3D X-ray Microscopy for Non-Destructive Failure Analysis of Chip-to-Chip Micro-bump Interconnects in Stacked Die Packages", *IEEE 24th Int'l Symp on the Physical and Failure Analysis of Integrated Circuits (IPFA),* Chengdu, China, Jul. 2017. doi:10.1109/IPFA.2017.8060111

[4] A. Gu, A. Andreyev, M. Terada, B. Zee, S. M. Zulkifli, Y. Yang, "Accelerate Your 3D X-ray Failure Analysis by Deep Learning High Resolution Reconstruction Paper," *Int'l Symp for Testing and Failure Analysis,* No: istfa2021p0291, pp. 291-295, Phoenix, AZ, Dec 2021.

[5] A. Gu, M. Terada, H. Stegmann, T. Rodgers, C. Fu and Y. Yang, "From System to Package to Interconnect: An Artificial Intelligence Powered 3D X-ray Imaging Solution for Semiconductor Package Structural Analysis and Correlative Microscopic Failure Analysis," *IPFA 2022,* Singapore

[6] Susan Li, "Failure Analysis Challenges for Chip Scale Packages," *ISTFA 2022,* Pasadena, California.

Original Published at 2023 IEEE International Symposium on the Physical and Failure Analysis of Integrated Circuits (IPFA)

A Breakthrough in Resolution and Scan Speed: Overcome the Challenges of 3D X-ray Imaging Workflows for Electronics Package Failure Analysis

Allen Gu, Gerhard Krampert, Susan Candell, Masako Terada,
Carl Zeiss Research Microscopy Solutions, 5300 Central Parkway, Dublin, CA 94568, USA

Thomas Rodgers
Carl Zeiss Microscopy GmbH, Rudolf Eber Str. 2, BG 41/1, 73447 Oberkochen, Germany

Abstract

Non-destructive 3D X-ray microscopy (XRM) has played an important role in advances of semiconductor packaging development and failure analysis [1-3]. Over the past decade, the IC industry has increasingly focused on packaging innovations to improve device performance and cost-effectiveness. The emergence of novel 2.5D, 3D and recent heterogenous integration packages challenges the existing X-ray imaging and characterization workflows because I/O interconnects such as small-volume solders and hybrid Cu-to-Cu bonds are more miniaturized in densely packed packages. In this report, we will introduce a new scintillator material coupled with a 40X objective lens (referred as 40X-P), integrated in an XRM detector system, capable of delivering better spatial resolution and contrast than the traditional Cesium Iodide (referred as CsI) scintillator based X-ray detector. Several commercial semiconductor packages will be imaged and analyzed with both the new 40X-P and a standard 40X objectives for comparison. We will also demonstrate that the data acquisition with 40X-P can be accelerated by a factor of four with a deep learning reconstruction method, improving its efficiency in failure analysis applications.

Introduction

Semiconductor packaging technologies have been the driving force to propel advances of electronics device performance, while traditional silicon downscaling has been slowing down. The IC packaging industry faces a paradigm shift in design, manufacturing, and inspection techniques to adopt more than Moore packaging innovations. Among many newly emerged interconnection techniques, fine pitch interconnection, 3D stacking, and solderless hybrid bonding are particularly attractive for the advantage to increase I/O density with the bridged size gap between Si and package. However, the IC industry faces the challenge to find an effective non-destructive solution for imaging these relentlessly miniaturized interconnects and defects.

3D XRM has become the preferred solution for semiconductor package failure analysis because of its non-destructive and high resolution capabilities. Unlike conventional computed tomography techniques, where spatial resolution solely relies on geometric magnification, XRM utilizes a unique two-stage magnification mechanism to achieve high resolution over large working distances. With both geometric and optical magnification, XRM enables submicron resolution across the normal range of semiconductor package sizes. XRM system resolution and contrast are defined by a variety of contributing factors such as source, detector, scan conditions, etc. In this paper, we focus on both the resolution and contrast improvement enabled by a new scintillator material coupled with a 40X objective lens. It is capable of delivering significantly better spatial resolution and contrast over a broader range of X-ray energies than the traditional CsI scintillator based detector. This is achieved via the higher density (i.e., higher average z-number) of the new scintillator material compared to CsI. Because of the heavy atom compositions, it converts high-energy X-ray photons to visible light better than the traditional CsI, making it better resolution and contrast even at high energies.

The first test vehicle was a commercially purchased 9x14x1.1 mm DRAM memory package with four layers of microbump and TSV stacks. The second test vehicle is a commercial 22x26x1 mm embedded multi-die interconnect bridge (EMIB) package with a heterogeneously integrated high-bandwidth memory and a graphics processor. We will demonstrate that the new 40X-P delivers better 2D and 3D resolutions and contrast of X-ray microscopic images on these test vehicles. In the previous studies, we reported the deep learning based reconstruction method can be used to speed up the scan throughput by a factor of four [4-6]. Here, we apply the reconstruction workflow to reduce the scan time of the 3D data acquired with the 40X-P objective.

Instrumentation and Setups

In a typical data acquisition with XRM, a sample rotates by 180 (± fan angle) or 360 degrees, and a set of projection images are acquired by an X-ray detector system. A scintillator screen coupled with an optical objective is utilized to convert X-ray photons to visible light, and the magnified projection images are captured by a CCD camera. These 2D images are mathematically reconstructed to 3D data. For the comparative studies, both 40X-P and standard 40X objective lenses were installed on a same turret for all imaging work. The standard procedures of beam alignment and objective calibration were followed.

Figure 1 shows the example 2D projections on a standard resolution target obtained with a standard 40X (Figure 1a) and the 40X-P (Figure 1b) objectives at 120 kV and a LE6 X-ray filter. Because of the superior performance at high energies of the new 40X-P, 500 nm spatial resolution was achieved. The measured modular transfer function of 40X-P only drops off at highest levels of resolution, indicating that the new objective maintains superior contrast in the high spatial frequency range. Although the peak performances of both objectives are achieved at a low energy, high energy performance is more critical in imaging high-density IC packages.

Results and Discussions

Because each projection contributes to the image quality of a reconstructed volume, it is important to optimize 2D X-ray projection views prior to 3D data acquisition. Figure 2 shows the two projection images on a commercially purchased DRAM package, which was not trimmed or prepared in the imaging work. Both images were acquired at 70 kV with a LE2 source filter at 0.49 µm/pixel resolution for a comparison.

The image acquired by the 40X-P objective in Fig. 2b looked much crispier than the image with a standard 40X objective in Figure 2a, especially on the edges of Cu pillars and microbumps. DRAM packaging architectures have utilized a small-volume soldering technique to stack multiple layers of dies through a thermocompression bonding process. The bond linethickness of ~15 µm and TSV with a diameter of 5 µm have been seen in advanced DRAM packages.

However, imaging small interconnects and internal defects of these packages has been challenging because of resolution limitations in microCT and XRM systems. Prior to the 40X objective tests, we used low-magnification objectives of 0.4X and 4X to precisely localize the scan region (Figure 3a) for the data acquisition with 40X objectives. With the X-ray imaging parameters in Figure 2, the sample was scanned with both 40X objectives.

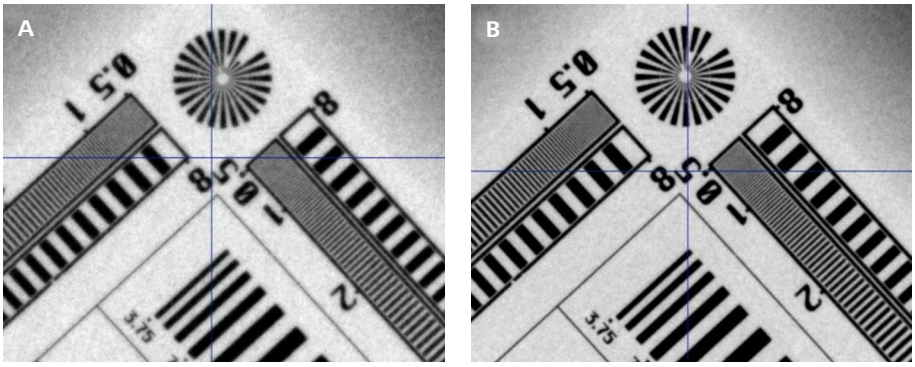

Figure 1 *Resolution and contrast performance comparison. A) A 2D projection view with a standard 40X objective lens at 120 kV X-ray energy and a LE6 filter. B) 2D projection view with the 40X-P at the same energy and filter. The test sample was a ZEISS standard resolution target.*

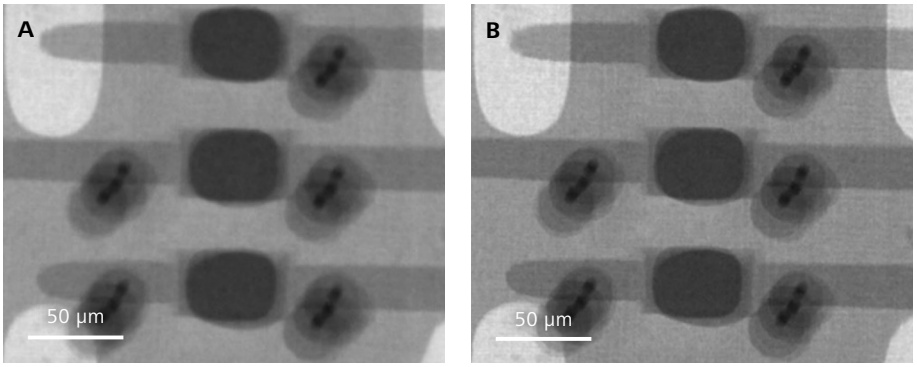

Figure 2 *Resolution performance comparison of 2D projections on the DRAM package sample. A) with a standard 40X objective lens at 70 kV and a LE2 filter. B) with the 40X-P at the same energy and filter.*

Figure 3c is a virtual cross-section image of TSVs and microbumps acquired with the 40X-P objective, clearly showing the resolution and contrast improvement over the image with a standard 40X objective (Figure 3b). Furthermore, the voids in microbump solders appeared much better defined than the image of the voids acquired by the standard 40X. The material phase separation can be clearly seen on the planar view acquired by 40X-P objective in Figure 3e, while the same virtual slice shows a blurry image on the phase separation in Figure 3d.

We reported a lab-based nanoscale tomographic technique to explore the applications of imaging semiconductor packages and back-end-of-line (BEOL) structures [7-8]. About 100 nm features can be effectively visualized, but the technique requires a significant sample preparation. Because the non-destructivity is highly valuated in failure analysis applications, we studied the 40X-P performance to image BEOL structures of an EMIB package, which are not among typical regions of interest with XRM. Figure 4b shows more promising resolution and contrast performance with the 40X-P objective, compared with the image performance by a standard 40X (Figure 4a). The metal lines and small submicron features are clearly resolved with greater certainty with the 40X-P objective than a standard 40X.

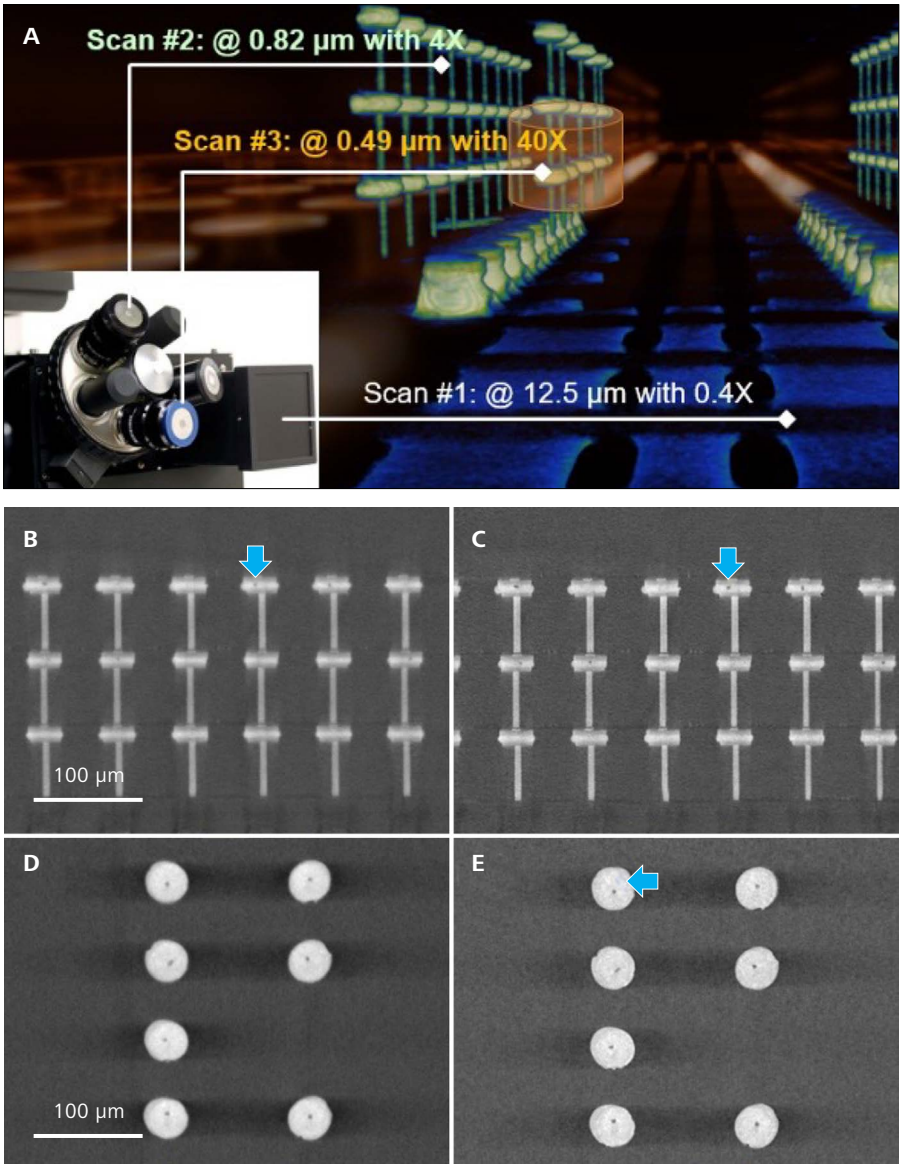

Figure 3 *A comparative study of the 40X-P objective to a standard 40X objective on the DRAM package sample. Two 3D tomographies with 40X objective were acquired at 0.49 µm/voxel. A) step-by-step zooming in scans with low mangification objectives of 0.4X and 4X, B) a cross-section view of the reconstructed volume acquired with a standard 40X objective, C) the corresponding cross-section with the 40X-P objective, D) a planar view of the reconstructed volume acquired with the standard 40X, and E) the corresponding planar view with the 40X-P objective.*

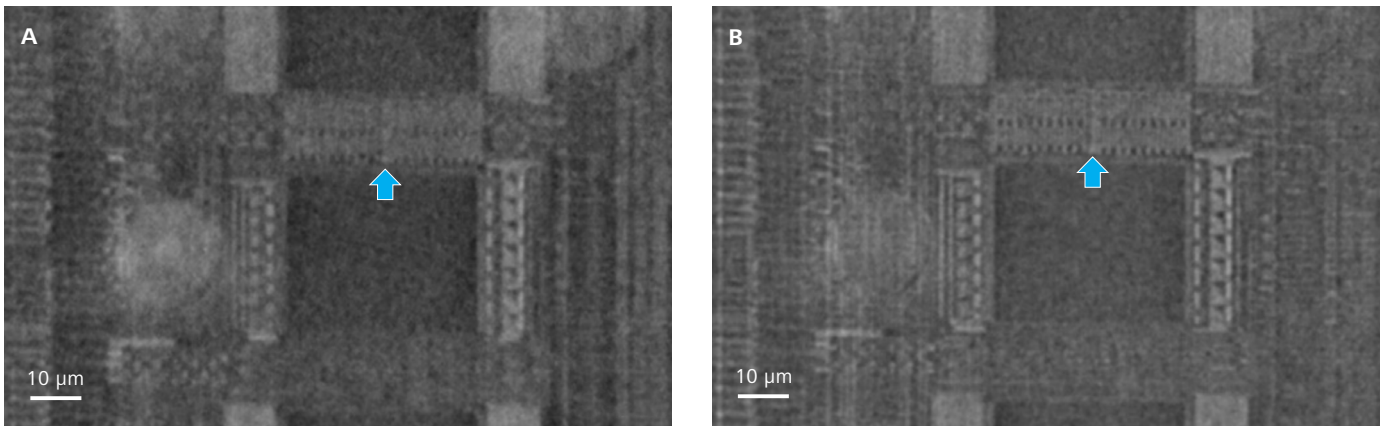

Figure 4 *Resolution and contrast performance comparison of the 40X-P objective with a standard 40X objective on the DRAM package sample. The tomography was acquired at 0.49 µm/vox resolution. A) a planar virtual slice of the reconstructed volume acquired with a standard 40X objective, B) the corresponding view with the 40X-P objective.*

EMIB packaging technique utilizes a small Si bridge to connect multiple dies. It is an alternative technique to 2.5D Si interposer packaging for its benefits on die placement flexibility and free of TSV process. An EMIB package was purchased through a commercial channel and the sample was not trimmed or prepared in the imaging work. Figure 5a shows the sample photo. A scan with 4X objective at 0.73 µm/vox resolution was performed to precisely localize a microbump region for the following 40X scans (Figure 5b). Figure 5c-f shows the 3D microscopic images acquired at 0.32 µm/voxel resolution with both 40X objective lenses. The virtual slice of the data acquired with the 40X-P objective shows the better resolution and contrast of the solder voids (Figure 5d) than with a standard 40X objective in Figure 5c. Even the smaller BEOL structures were resolved more clearly in the image acquired with the 40X-P objective. The example planar view in Figure 5f revealed the surface detail of metal traces, indicating the image obtained by the 40X-P objective delivers better resolution and contrast than the standard 40X objective.

To demonstrate that this new 40X-P detector can be efficiently used in X-ray failure analysis workflow, we utilized the deep learning reconstruction method reported previously [4-6] to improve the scan throughput while maintain the image quality. The standard Feldkamp-Davis-Kress (FDK) reconstruction provides accurate and fast reconstruction, but it is sensitive to photon starvation and resulting images are prone to noise and under-sampling artifacts. For example, a typical data acquisition with a 40X objective lens requires an overnight scan with the FDK reconstruction for high image quality. In a 3.5 hour scan with the 40X-P objective and FDK reconstruction, the detail of microbump and BEOL structures has not been clearly revealed due to high noise level (Figure 6a).

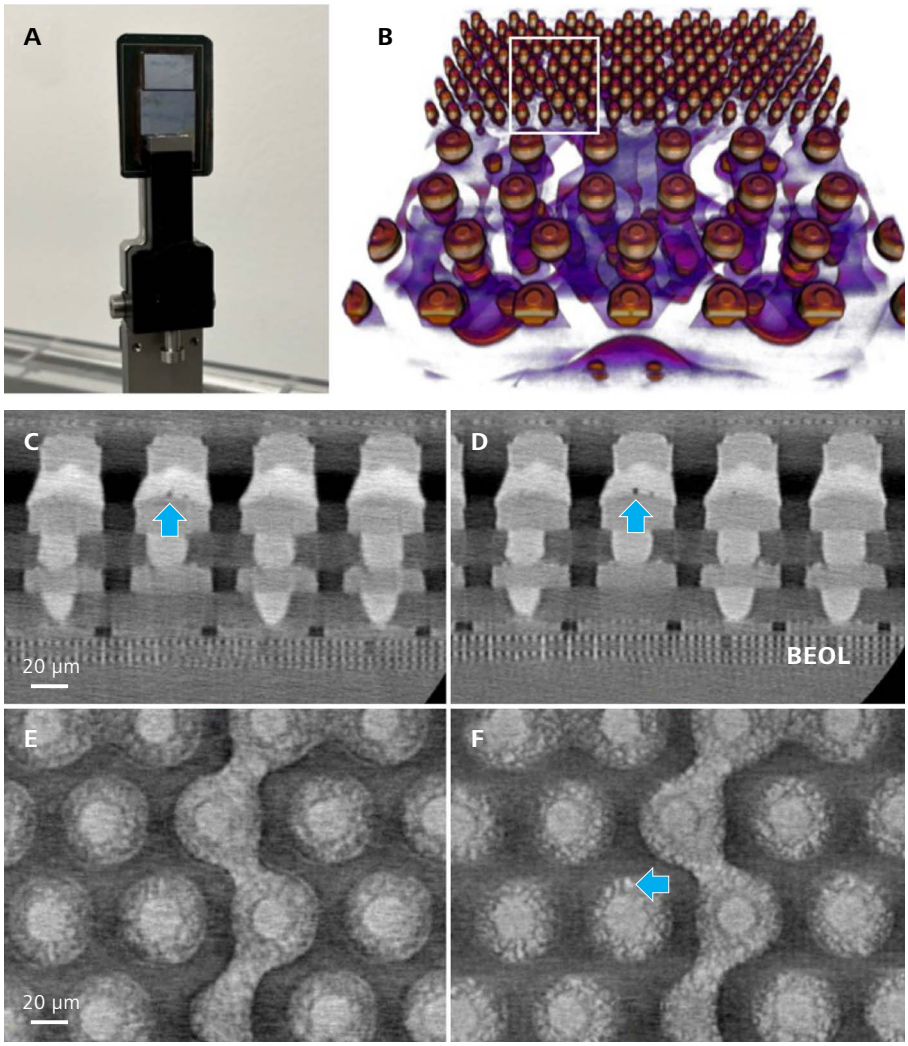

Figure 5 *A comparison of the 40X-P objective to a standard 40X objective on the EMIB package sample. The images were acquired with both 40X objectives at 0.32 µm/vox resolution. A) photo of the sample, B) the image was acquired with 4X at 0.73 µm/vox for localizing 40X scans, C) a cross-section view of the reconstructed volume acquired with a standard 40X objective, D) the corresponding cross-section view with the 40X-P objective, E) a planar view of the reconstructed volume acquired with a standard 40X, and F) the corresponding cross-section view with the 40X-P objective.*

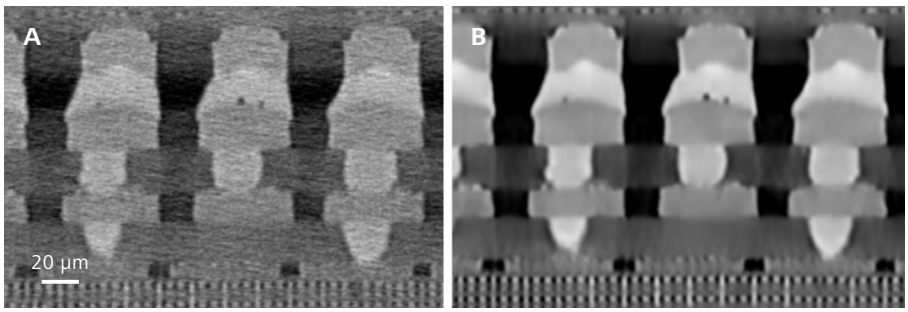

Figure 6 *A comparative study of the deep learning reconstruction result to the standard FDK reconstruction. The tomography was acquired at 0.32 µm/vox resolution with the 40X-P objective. A) a virtual slice from a 3.5 hour scan with the standard FDK reconstruction. B) the same virtual slice from a 3.5 hour scan with the deep learning reconstruction method.*

By contrast, the 3.5 hour scan with the deep learning reconstruction clearly shows the improved image quality with the same scan time (Figure 6b). The result shows that the new 40X-P detector can be efficiently used for failure analysis workflows with unparalleled resolution and contrast.

Conclusion

The impacts of innovative packaging technologies have been seen across advanced semiconductor packages. The failure analysis community always carves for more effective and efficient non-destructive solutions for solving root cause analysis challenges in these complex packages. We demonstrated the breakthrough in resolution and contrast is enabled with a new scintillator material based X-ray detector in XRM. Because of its superior performance at higher energies over the traditional CsI scintillator based detector, it can be used in imaging high-density semiconductor packages. With the deep learning reconstruction workflow, the scan speed can be improved while maintaining the unprecedented resolution and contrast.

References

[1] L. Mirkarimi, A. Gu, L. Hunter, G. Guevara, M. Huynh, R. Katkar, "X-ray Microscopy and Root Cause Analysis in Electronic Packaging", Proc 41st Int'l Symp for Testing and Failure Analysis, Portland, OR, Nov. 2015, pp. 430-435. doi: 10.31399/asm.cp.istfa2015p0430

[2] S. M. Zulkifli, B. Zee, W. Qiu, A. Gu, "High-Res 3D X-ray Microscopy for Non-Destructive Failure Analysis of Chip-to-Chip Micro-bump Interconnects in Stacked Die Packages", IEEE 24th Int'l Symp on the Physical and Failure Analysis of Integrated Circuits (IPFA), Chengdu, China, Jul. 2017. doi:10.1109/IPFA.2017.8060111

[3] A. Gu, J. Auyoong, "3D Measurement Workflow for Packaging Development and Production Control Using High-Resolution 3D X-ray Microscope", 2018 IEEE 20th Electronics Packaging Tech Confer (EPTC), Singapore, Dec. 2018. doi:10.1109/EPTC.2018.8654390

[4] M. Andrew, R. Sanapala, A. Andreyev, H. Bale, C. Hartfield, "Supercharging X-ray Microscopy Using Advanced Algorithms", Microscopy and Analysis, pp17, Nov/Dec 2020

[5] A. Gu, A. Andreyev, M. Terada, B. Zee, S. M. Zulkifli, Y. Yang, "Accelerate Your 3D X-ray Failure Analysis by Deep Learning High Resolution Reconstruction Paper," Int'l Symp for Testing and Failure Analysis, No: istfa2021p0291, pp. 291-295, Phoenix, AZ, Dec 2021

[6] A. Gu, M. Terada, H. Stegmann, T. Rodgers, C. Fu and Y. Yang, "From System to Package to Interconnect: An Artificial Intelligence Powered 3D X-ray Imaging Solution for Semiconductor Package Structural Analysis and Correlative Microscopic Failure Analysis," IPFA 2022, Singapore

[7] C. Schmidt, S. Kelly, Y. Wang, S.T. Coyle, M. H. Shearer, "Novel sample preparation and High-Resolution X-ray tomography for Package FA," IEEE 24th Int'l Symp on the Physical and Failure Analysis of Integrated Circuits (IPFA), Chengdu, China, Jul. 2017

[8] C. Schmidt, L. Lechner, I. DeWolf, S. W. Kim, E. Beyne, "Novel failure analysis techniques for 1.8 µm pitch wafer-to-wafer bonding," IEEE 68th Electronic Components and Technology Conference, San Diego, CA, May 2018.

Originally Published at ICSJ 2022: Proceedings from 11th IEEE Components, Packaging and Manufacturing Technology (CPMT) Symposium Japan (ICSJ)

Targeted Sample Preparation and Analysis of Advanced Packaging using Correlated X-ray Microscopy and LaserFIB

Seeing beyond

Vignesh Viswanathan
Research Microscopy Solutions, Carl Zeiss Pte Ltd, Singapore, Singapore

Takehide Oda, Etsuo Maeda, Chisato Yamamoto
Research Microscopy Solutions, Carl Zeiss Co., Ltd., Tokyo, Japan

Longan Jiao
Research Microscopy Solutions, Carl Zeiss (Shanghai) Co., Ltd., Shanghai, China

Abstract

X-ray microscopy and femtosecond (fs) laser integrated FIB-SEM are combined in a workflow to guide precise and targeted sample preparation to enable functional testing and fault isolation without damaging the package and IC.

Introduction

Emerging technologies such as AI, 5G, IoT, wearables, cloud, computing, and autonomous vehicles hold great promise for improvement and transformation of human lives globally. In today's More-than-Moore era, advanced packaging has emerged as a critical enabler for these next generation of electronic devices. System level performance improvements through heterogeneous integration has added more functionality while improving the cost-performance gaps. Developments in various materials, processes, and architectures for 2.5D and 3D packaging has enabled high density interconnects with shrinking dimensions and pitch which is essential for continued scaling in performance and integration of various devices at lower costs.

As the complexity of electronic packages continues to increase, so do the challenges in characterization during process development and failure analysis (FA). Traditionally, FA workflow in IC packaging begins with the electrical and functional testing of the device followed by incoming optical and 2D X-ray inspection. Subsequent fault isolation using multiple tools and techniques have become necessary starting with curve tracing, TDR, high resolution, non-destructive imaging using SAM, X-ray CT, and IR imaging followed by physical analysis using mechanical and focused ion beam (FIB)-based cross-sectioning for visualizing and characterization of defects, Figure 1. [1]

Once the fault isolation is completed and a failure site has been localized, high-resolution imaging techniques such as 3D X-ray microscopy (XRM) can visualize defects and guide sample preparation for physical analysis to disclose defects for root cause investigation [2, 3]. However, the region of interest (ROI) may be several hundreds of microns (µm) or millimeter (mm) deep into the package which requires removal of large volume of material with high accuracy in the microns or better range. Conventional techniques such as mechanical cross-section enable large cross-section preparation but are slow and have limited accuracy. FIB using liquid metal ion source or plasma ion source is very precise and effective in preparing cross-sections in the hundreds of microns cubic volume which would still need long preparation times to access deep structures (hours to days). Laser ablation using ultra-fast pulsed lasers have been adopted as stand-alone and integrated into FIB systems which allows large volume removal (mm^3) at high throughput (minutes to hours) [4-7].

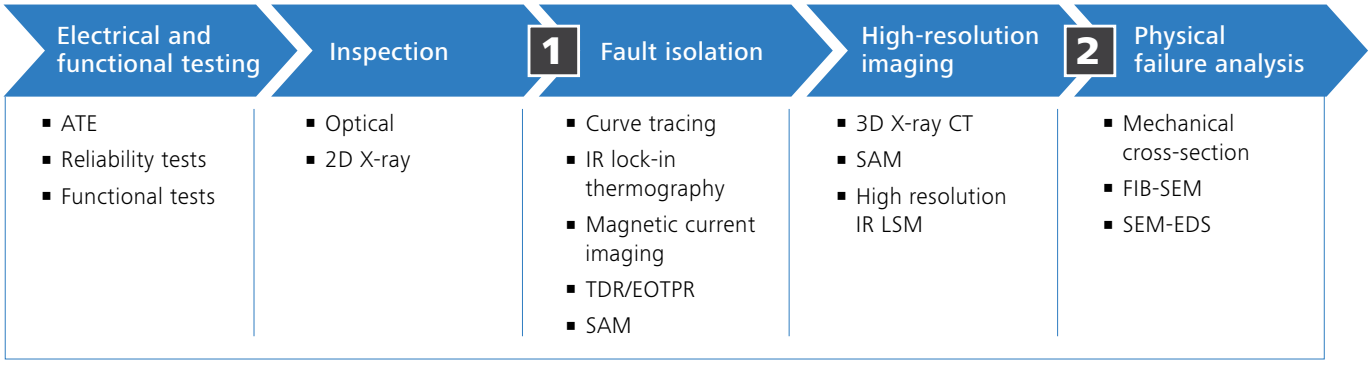

For targeting sub-surface and buried features, an XRM-guided workflow for sample preparation through integrated laserFIBs has already demonstrated high precision and high throughput sample preparation in 2.5D packaging and display [8-11]. Besides large volume removal, the ability to access deeply buried structures with high precision can also be used to selectively sever electrical wires and connections to simplify and isolate complex circuitry during fault isolation.

In advanced packages with high IO and complex interconnect structures, localization of tiny defects by electrical curve tracing, TDR, or lock-in thermography can be challenging. Finding these failures in complex packages such as system-in-package, multi- stack dies and package-on-package devices with several functional components can be quite time consuming. Deduction by elimination would require disconnecting or breaking the electrical connectivity in parts of the circuitry without affecting any other component which can be a challenge. This would require a precise and selective technique to break the interconnects and wires while retaining all other functionalities of the device.

In this work, we apply a workflow combining a non-destructive 3D X-ray microscopy that guides the sample preparation using a FIB integrated with an fs laser with high precision for fault isolation in 3D packages.

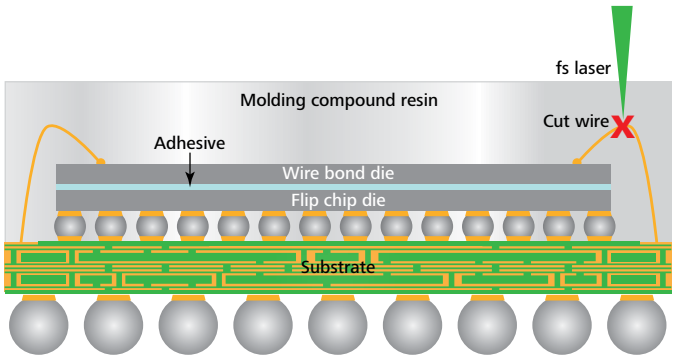

Figure 2 *Schematic illustrating how wire bond can be cut to isolate functions from the top die during functional testing and fault isolation*

Methods

A. Sample Preparation

For the demonstration of this workflow, we extracted a base band modem IC from the motherboard of a mobile phone, which is a 3D package consisting of one flip-chip die (baseband processor) connected to the substrate through solder bumps and another die (memory and/or analog) with wire bonds. Upon preliminary inspection, no damage to the internal structures was observed.

B. Workflow

In 3D packages, electrical connections going to the different modules may have complex circuitry that could lead to challenging fault isolation routines to identify the failure sites. In such 3D packaging, it would require deactivating certain features or parts of the circuit to isolate some components and determine failure sites with higher accuracy. The ability to selectively break an interconnect or wire without damaging the chip for functional testing can be achieved if they are accessible either through the molding compound or through other protective packaging materials as highlighted in Figure 2.

The workflow combines two techniques, a high-resolution non-destructive 3D X-ray microscopy and an fs laser integrated FIB-SEM. In this work, we utilize ZEISS 620 Xradia Versa and ZEISS Crossbeam laser 550 to perform the analysis. Figure 3 illustrates the process and steps involved. The sample is scanned at low resolution to obtain an overview of the entire package and interconnect structure to check for defects or anomalies. This information may be available from other fault isolation techniques or known data and may be skipped. Once the region of interest (ROI) is identified, this must be referenced to a unique feature that is visible and accessible for imaging either by SEM or optical methods on the surface. Hence, the top surface above the ROI is marked to add fiducials for easy reference to the sub-surface feature. The package is scanned again using the X-ray microscope at sufficient resolution to capture both ROI and the surface fiducials to localize the ROI with respect to the surface fiducials.

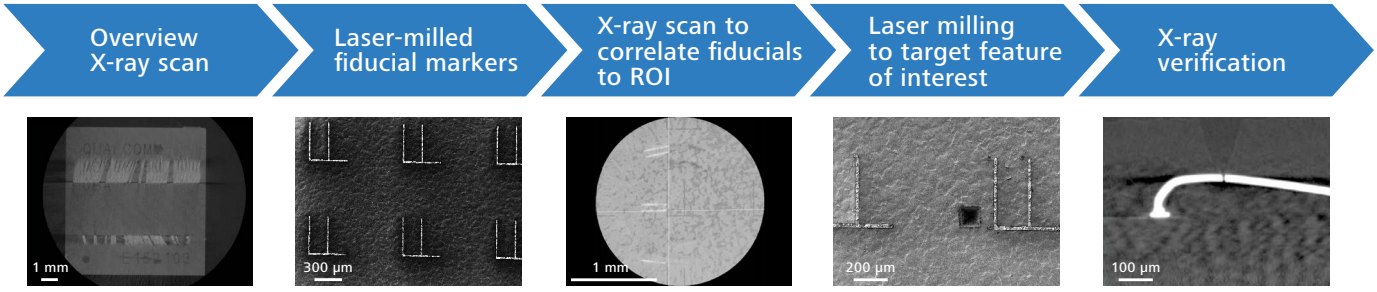

Figure 3 *Sample preparation workflow process using 3D X-ray guided laser milling of interconnects for fault isolation*

Subsequently, the fs laser is used to perform a precise fine cut on the desired wire or interconnect to isolate features or parts of the circuitry. The sample is again checked using the X-ray to determine if the precise cutting is sufficient or successful for further fault isolation.

In this example we demonstrate that the 20 µm wide wire that is 150 µm deep can be precisely cut with the laser without decapsulating or damaging any part of the die and other interconnects or neighboring wires. To improve the laser milling accuracy, a calibration step is performed to determine the parameters for accurate positioning and laser milling depth. Once the calibration is performed, thelaser parameters can be replicated on additional wires or on other samples made of similar materials. The results are presented in the next section.

Results

The first experiment is performed to determine the optimal milling parameters, Figure 4. The second experiment is performed targeting a single wire to demonstrate precision and replication of the milling parameters on other sites, Figure 5. The overview X-ray scan is acquired in 28 minutes at 100kV, 14W and 12 µm/voxel. The low-resolution fast scan is sufficient to observe the internal structure of the devices and layout of the interconnects and wires. The sample is mounted on a carbon stub which allows transfer of the sample between the XRM and LaserFIB. Subsequently, the sample is transferred to the LaserFIB to generate fiducial markers on the top right. The Crossbeam laser 550 operates with a separate chamber for laser milling and has micron scale accuracy with a registration process between the SEM and laser. The laser milling is performed at 4W with a pulse frequency of 10 KHz and milling time is 1 second. The fiducial markers are 20 µm wide and over 1.2 mm x 1.2 mm. The sample is scanned again with the XRM at higher resolution at 2 µm/voxel at 100kV and 14W in 2 hours.

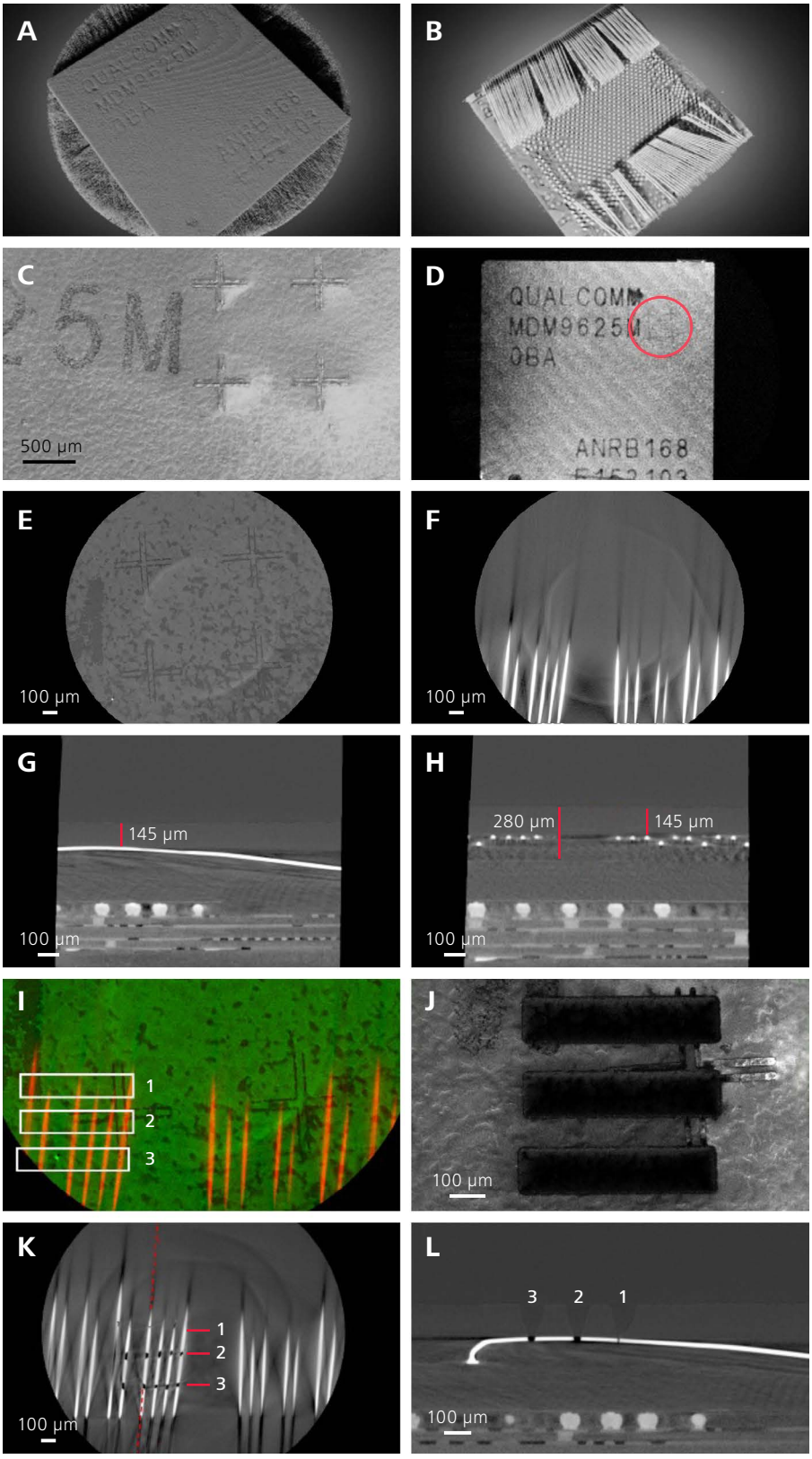

Figure 4 *A) Overview X-ray scan of chip showing top molding compound surface and B) internal wires and flip chip bumps. C) SEM image after laser marking of fiducials. D) XRM overview showing position of fiducials highlighted by red circle. E) Higher magnification XRM scan virtual cross-section of the fiducials and F) underlying wires. G) and H) Distance of the wires and chip from the top surface is measured to be 145 µm and 280 µm respectively. I) Top surface (in green) with laser fiducuals is overlayed with wires (in orange) and the position of laser milling test patterns 1,2 and 3 with varying doses are shown. J) SEM image after laser milling. K) XRM scan showing virtual cross-section on top of the wire and L) virtual cross-section view of wires cut corresponding to the 3.*

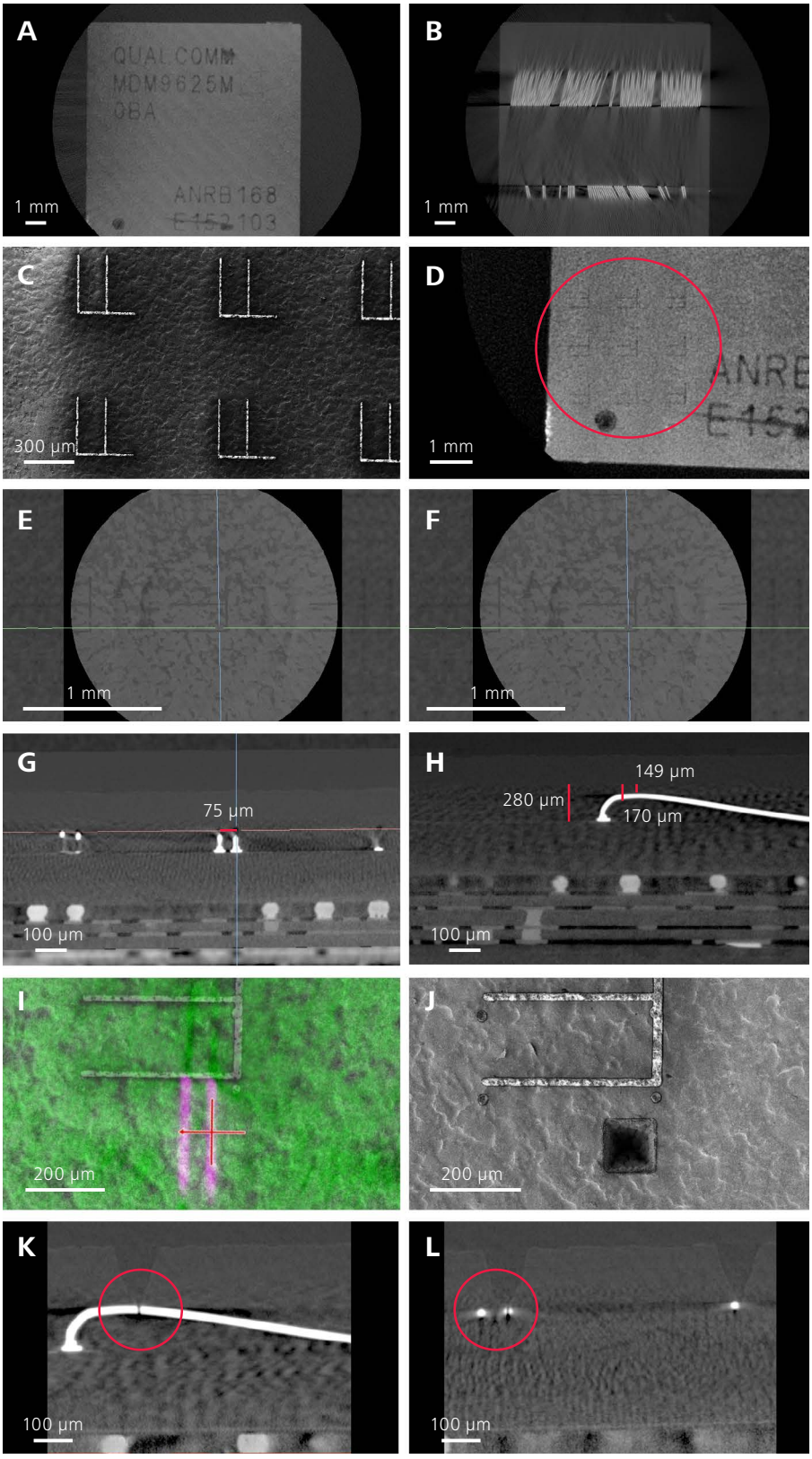

Figure 5 *A) Overview X-ray scan of chip showing top molding compound surface and B) internal wires and flip chip bumps. C) SEM image after laser marking of fiducials. D) XRM overview showing position of fiducials. E) Higher magnification XRM scan virtual cross-section of fiducials and F) underlying wires. G) The distance of wire from neighboring wire and H) distance of wire from top surface and distance of chip from the top is measured to be 149 µm and 280 µm respectively. I) top surface (in green) with laser fiducuals is overlayed with the wires (in pink) and the position of laser milling is highlighted by the crosshair. J) SEM image after laser milling 100 x 100 µm square targeting 150 µm deep wire. K) XRM scan showing virtual side view of cut wire while L) maintaining neighboring wire.*

Now both the ROI and fiducial markers are captured. The position of the wires with respect to the laser milled surface fiducial markers can be determined by overlaying the two virtual cross-sections. The wire is 145 µm below the surface and has a diameter of about 20 µm. The die is 280 µm below the surface giving a clearance of about 115 µm from the bottom of the wire. Since the material information is not known, the laser milling parameters are to be optimized with a dose test such that the milling only cuts the wire and does not penetrate deeper to damage the die. A series of rectangles (labelled 1, 2 and 3) 100 µm x 100 µm is milled at 4W with a frequency of 10 KHz and speed of 20 mm/sec while varying additional parameters to control the milling depth to determine the optimal conditions for the laser milling. The milling pattern cuts multiple wires providing several data points to check for repeatability and local variations in the materials due to fillers or additional components. The milling takes less than 20 seconds to complete. The sample is then scanned again in the XRM at 2 µm/voxel at 100kV and 14W in 2 hours to check the depth of the laser cuts. It can be observed that the dose in rectangle 1 is insufficient to cut the wire reliably while the dose in rectangles 2 and 3 cut the wires and do not damage the die below. The optimal dose is chosen to be dose 2.

The same workflow is now followed to target a single wire in another area of the chip as shown in Figure 5. Previous X-ray overview scans provide low resolution position information to laser mill surface fiducial marks on the lower left corner of the chip. Laser milling of fiducials follow earlier recipe and are completed in less than 1 second. Higher resolution X-ray scan at 2 µm/voxel is required to obtain accurate positioning of the target wire. The wire is about 150 µm from the top surface and the nearest wire is at a pitch of 75 µm. The overlay of the X-ray image with the fiducials and wires are aligned with the SEM image to provide a precise location of the wire, Figure 5I.

Now a 100 µm x 100 µm rectangle is positioned precisely and milled with the laser following the earlier recipe. The milling is completed within 20 seconds. The final X-ray scan verifies that the laser cut precisely targets the wire of interest and doesn't damage the neighboring wire or the die below indicating the workflow can be employed for precise and targeted sample preparation.

Discussion

In this work, the recipe is repeatable at different locations within the same sample and for similar packages using the same molding compound materials. However, the variations arising due to the presence of filler materials and other additives are not thoroughly studied and would need further optimization. The gaussian profile of the laser beam introduces a side wall taper of close to 15 degrees which adds requirements on the minimum opening area at the top surface to completely cut the wire and this depends on the depth of the interconnect from the surface. The entire workflow takes 5 hours and can be completed in 6-8 hours including data reconstruction and preparation time in between steps. Further functional testing of the chip is required to validate the proposed method and is part of the future work.

Conclusion

A novel correlative workflow using LaserFIB and 3D XRM techniques is presented for targeted sample preparation for fault isolation in 3D BGA packages consisting of wire bonds and flip chip devices. The case study presented targets an interconnect wire connecting the top die in the 3D package to isolate part of the circuit / device for functional testing and fault isolation. The 620 Versa 3D XRM was used to scan and identify the interconnects and features and correlate with surface features patterned on the sample using the Crossbeam 550 fs-Laser FIB-SEM for precise targeting and sample preparation. The wire was cut precisely without damaging neighboring wires or the die while retaining most of the package for further testing. The entire process from feature identification until the wire milling and isolation of the circuit is completed in 8 hours highlighting the throughput and precision capabilities of this streamlined workflow which can open new capabilities in the fault isolation and failure analysis of advanced packages.

Acknowledgement

The authors would like to acknowledge the support from ZEISS Microscopy Customer Centre Tokyo in providing the microscopes and tools used to develop this workflow.

References

[1] Pacheco, M., Wang, Z., Skoglund, L., Liu, Y., Medina, A., Raman, A., Dias, R., Goyal, D., and Ramanathan, S., "Advanced Fault Isolation and Failure Analysis Techniques for Future Package Technologies." Intel Technology Journal, 9(4) 2005.

[2] Sylvester, Y., Hunter, L., Johnson, B. and Estrada, R., "3D X-ray microscopy: A near-SEM non-destructive imaging technology used in the development of 3D IC packaging," 2013 IEEE International 3D Systems Integration Conference (3DIC), 2013, pp. 1-7.

[3] Nair Gourikutty S.B, Chow, Y. M., Alton, J., Umralkar, R.B., Bai, H., Chua, K.K., Bhattacharya, S., "Defect Localization in Through-Si-Interposer Based 2.5D ICs," 2020 IEEE 70th Electronic Components and Technology Conference (ECTC), 2020, pp. 1180-1185.

[4] Stegmann, H., Dömer, H., Cai, H., Rosenkranz, R. and Zschech, E., "Efficient target preparation by combining laser ablation and FIB milling in a single tool," 2011 Semiconductor Conference Dresden, 2011, pp. 1-4.

[5] Randolph, S. J., Filevich, J., Botman, A., Gannon, R., Rue, C., & Straw, M. "In situ femtosecond pulse laser ablation for large volume 3D analysis in scanning electron microscope systems" Journal of Vacuum Science & Technology B, Vol. 36, No. 6 (2018), 06JB01.

[6] Tuček, M., Blando, R., Váňa, R., Hladík, L. and Oboňa, J. V., "Speeding up large-scale failure analysis of semiconductor devices by laser ablation," 2020 IEEE International Symposium on the Physical and Failure Analysis of Integrated Circuits (IPFA), 2020, pp. 1-3.

[7] Tordoff, B., Hartfield, C., Holwell, A.J. et al. "The LaserFIB: new application opportunities combining a high-performance FIB-SEM with femtosecond laser processing in an integrated second chamber," *Appl. Microsc.* Vol. 50, No. 24 (2020)

[8] Hartfield, C., Kaestner, M., Mueller, S., Atkinson-Mora, J. and Schullmeyer, I., "A new approach for rapid analysis of buried 2.5/3D package structures", Chip Scale Review Vol. 24, No. 3 (2020) pp. 39-42.

[9] Kaestner, M., Mueller, S., Gregorich, T., Hartfield, C., Nolan, C., Schulmeyer, I., "Novel workflow for high-resolution imaging of structures in advanced 3D and fan-out packages", China Semiconductor Technology International Conference (CSTIC) (IEEE, Shanghai, 2019), pp. 1–3.

[10] Leslie, N., Lai, B., Lee, H., Lee, M., Kang, C.H., Patakova, Z., Zelenka, F., and Varslot, T., "Addressing Failures in Advanced Packaging Through a Correlative Workflow" International Symposium for Testing and Failure Analysis (ISTFA), 2020, pp. 17-19.

[11] Viswanathan, V., Jiao, L. and Hartfield, C., "Developments in Advanced Packaging Failure Analysis using Correlated X-ray Microscopy and LaserFIB", 2021 IEEE 23rd Electronics Packaging Technology Conference (EPTC), 2021, pp. 80-84.

Originally Published at ISTFA 2024: Proceedings from the 50th International Symposium for Testing and Failure Analysis Conference

Correlative Microscopic Workflow Powered by Artificial Intelligence to Accelerate Failure Analysis of Next-Generation Semiconductor Packages

Seeing beyond

Yu-Jen Chang, Cheng-Hsin Liu, Yi-Sheng Lin, Chen-Chao Wang
Advanced Semiconductor Engineering
Nicky Liu, Bessy Chiu, Allen Gu
ZEISS Microscopy

Abstract

Over the past decade, the semiconductor industry has increasingly focused on packaging innovations to improve device performance, power efficiency, and reduce manufacturing cost. The recent heterogeneous integration offers an attractive solution in advanced IC packaging because it enables the integration of diverse functional components, such as logic, memory, power modulator, and sensor on a single package platform. However, the adoption of the emerging structures, materials, and components in advanced packages has challenged existing fault isolation and analysis techniques. One of the major challenges is the limited accessibility to defects because fault regions are often located deep within devices. Without high-accuracy positional information of a defect, physical cross-sectioning and FIB polishing may alter or destroy the evidence of root causes.

A non-destructive microscopic approach is preferred to map defective sites and surrounding structures. However, this method is limited by spatial resolution, especially for analyzing novel submicron interconnects such as fine pitch microbumps, redistribution layers (RDLs), and hybrid bonds. In this paper, we report an AI powered correlative microscopic workflow, where non-destructive X-ray imaging, FIB polishing, and high-resolution SEM analyzing techniques are combined to solve the accessibility problem. Because 3D X-ray imaging may take a larger fraction of the time span over the entire workflow, a deep-learning based reconstruction method was applied to accelerate data acquisition. Several next-generation packages, fan-out wafer-level package (FOWLP) and hybrid bonds with sub 10 µm pitch, were used as the test vehicles to demonstrate the workflow performance and efficiency.

Introduction

Next generation packaging technologies present significant challenges to the mainstream packaging and failure analysis techniques. The ability to localize and visualize a defect prior to physical failure analysis (PFA) is no longer straightforward. FOWLP offers diverse benefits such as increased external I/Os, integration of thin dies, and improved fine-pitch interconnections. However, challenges have risen in FOWLP failure analysis due to its complex package structure, thin die handling, and dense layer-to-layer connectivity. In new heterogeneously-integrated packages, hybrid bonding provides a solution for sub 10 µm pitches by using solderless Cu-to-Cu bonds to connect stacked dies. It generates superior interconnection density, enabling 3D, 2.5D packages, and advanced memory cubes. However, hybrid bonding relies on pristine surface quality and precise alignment to ensure bonding quality, strength, and reliability. The failure mechanisms and root causes on these two packages and interconnects are not completely understood.

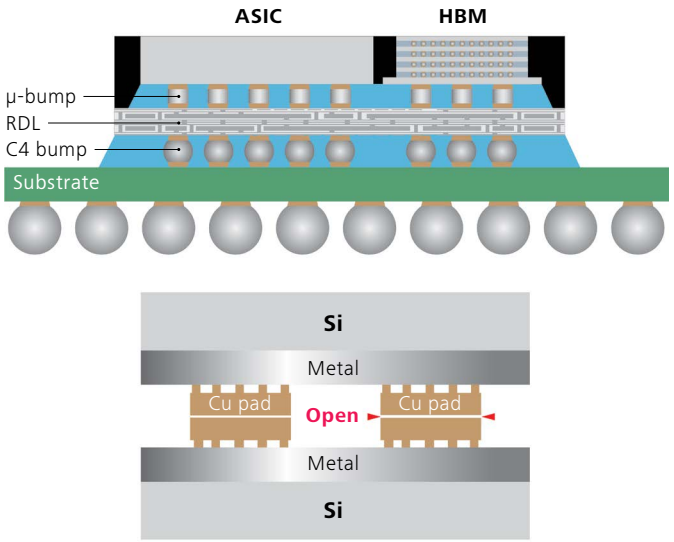

Figure 1 *The schematics of the test vehicles: fan-out wafer-level package (top) and hybrid bond package (bottom).*

3D X-ray microscopy (XRM) is widely utilized as an effective high-resolution and non-destructive imaging and analysis tool in package-level failure analysis.[1-4] With a recently developed deep learning reconstruction method, X-ray scan speed can be accelerated by a factor of four. [5-6] With the assistance of acquired 3D XRM dataset, failure analysts can navigate through the entire package volume to identify the specific regions and failures of interest. This makes the subsequent cross-sectioning more effective than the conventional broad ion beam polishing, where the actual location of a defect may be missed because no 3D navigational information is available. We have demonstrated that the integration of laser ablation with focused ion beam (FIB) techniques has enabled rapid preparation of site-specific cross-sections with extremely high precision.[7-8] In this paper, we report a three-step PFA process dedicated to analyze fine structures and defects in several FOWLP and hybrid bonding packages with high accuracy. Firstly, a semiconductor package is imaged with high-resolution 3D XRM, and the AI-powered reconstruction is used to accelerate scan speed. Secondly, X-ray images are aligned and correlated with SEM images based on FIB cut fiducial marks on a package surface. This is the main step in the correlative workflow, where these two instruments are connected through the shared coordinates of the defect. Finally, the FIB polished surface is imaged and analyzed with FE-SEM.

Results

FOWLP microbumps

A FOWLP package with the µbump inter-connection issue was sent in to test the correlative workflow. An electrical test was performed and initially concluded that the bad connectivity on a specific bump may be the root cause of the open circuit (Figure 2a). In order to validate the observation, the proposed correlative workflow was performed.

Figure 2b shows several FIB cut fiducial marks for subsequent registration. It took 18 minutes to mill the trapezoid of 20x30 µm opening and 20 µm deep, with FIB current of 30 nA at 30 kV. A 30 µm radius circle was created with FIB current of 30 nA for 12 minutes.

Although a 3D X-ray scan is typically performed in the workflow, here we utilized a single X-ray projection image of the thin package for saving scan time, because it reveals good enough contrast for registration purpose.

Figure 2c shows both fiducial marks were visualized with the fast X-ray projection. The phase-contrast image was acquired with 0.26 µm/pixel resolution at 70 kV for 20 sec exposure time. Figure 2d is slightly zoomed-out image that shows the target µbump near to the fiducial mark. The X-ray propagation phase contrast is the alternative method to the more popular absorption contrast. In a typical phase contrast imaging setup, X-ray photons pick up the difference that exists in X-ray refractive index at the air-silicon interfaces.

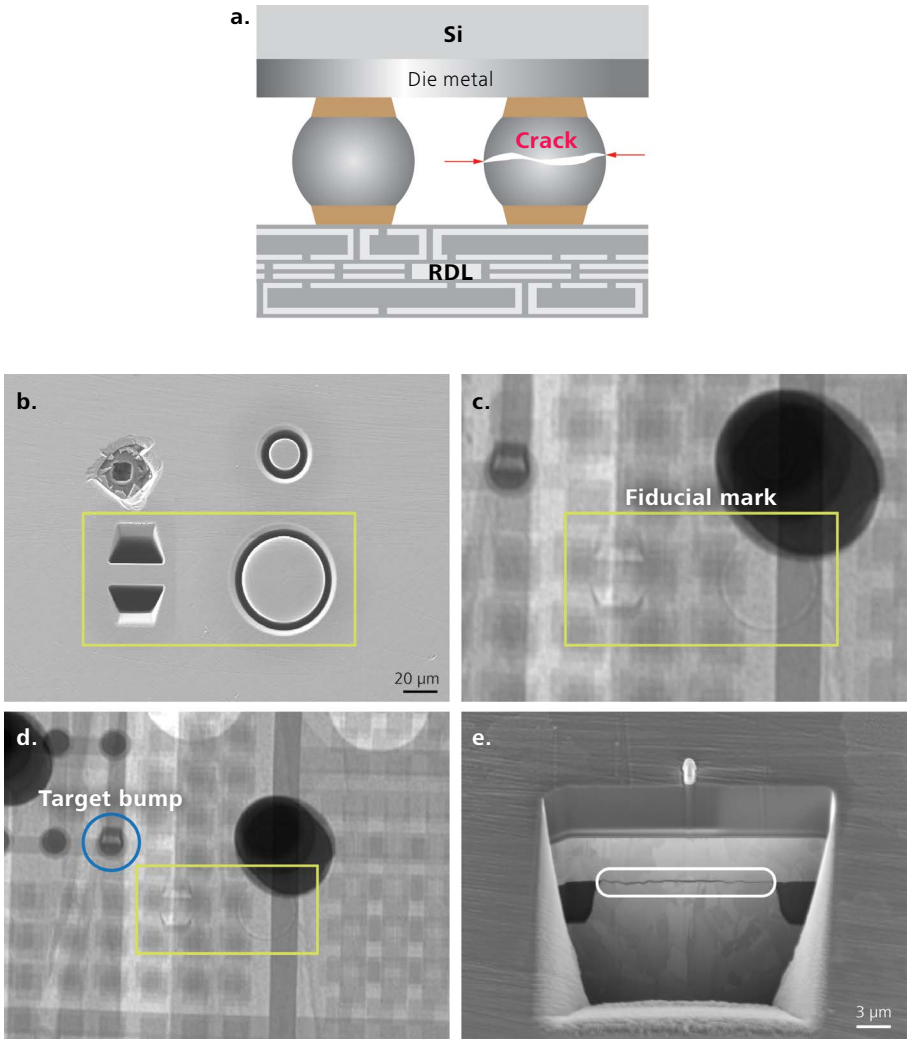

Figure 2 *The case study of FOWLP µbump: a) the schematics of the package structures shows possible defective microbump. b) FIB cuts of several geometric features (inside the green box) used as fiducial marks. c) 2D X-ray phase contrast image shows the fiducial marks. d) A large field of view X-ray image shows both the target bump and fiducial mark. e) ~100 nm bump cracks revealed during the FIB cutting and SEM imaging workflow.*

With the highlighted interfaces, the edges of the FIB-cut fiducial marks can be differentiated easily without investing long time for 3D X-ray scans. In this case, it only took ~200 sec for the phase contrast imaging. Using the alignment software configured within the FIB system, the exact bump location was identified. We performed a FIB cross-sectioning and polishing. Figure 2e shows ~100 nm bump cracks that would nothave been detected with X-ray imaging. The CTE mismatch between silicon and the PCB was the root cause of the bump crack.

FOWLP RDL

RDL plays a critical role in FOWLP packages for redistributing electrical signals between dies and external interconnects. Less than 2x2 µm fine pitch RDLs in next-generation WLP devices may have several challenges for failure analysis because of process uniformity, high aspect ratios, and alignment accuracy.

For a robustness test of RDLs and underfills, we used the proposed correlative workflow to evaluate how underfill cracks may have an impact on RDL metal lines underneath. Figure 3a-b shows the case study of RDL layers (2x2 µm) in a FOWLP package. The fiducial mark "ASE" was cut by FIB with 30 kV and 30 nA shown in Figure 3c. It took about 20 minutes for ~20 µm deep feature. The underfill cracks were visualized on the same micrograph. A 3D X-ray scan with a standard reconstruction at 0.83 µm resolution was followed for 3.6 hour scan time (Figure 3d).

Cycle time is critical in semiconductor package-level failure isolation and analysis. To improve 3D X-ray scan throughput which is usually a bottle-neck of the analysis workflow, we used the deep-learning based reconstruction method described in reference.[5-6]

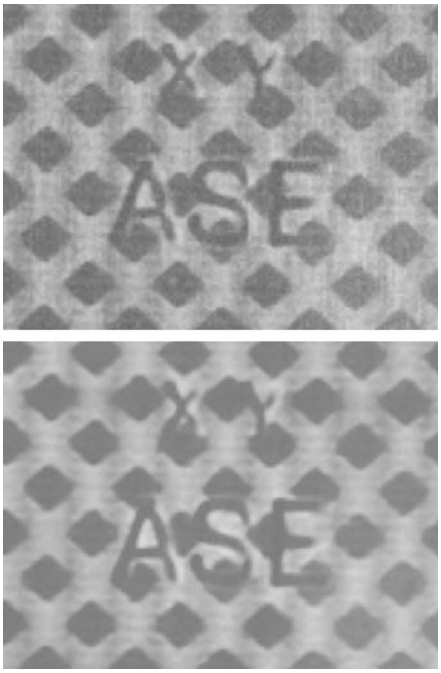

Figure 4 *A comparison of the standard FDK with the deep learning-based reconstruction. a) the virtual slice shows the fiducial mark acquired by FDK for 3.6 hours. b) the same slice acquired for 0.9 hours and reconstructed with the deep learning reconstruction.*

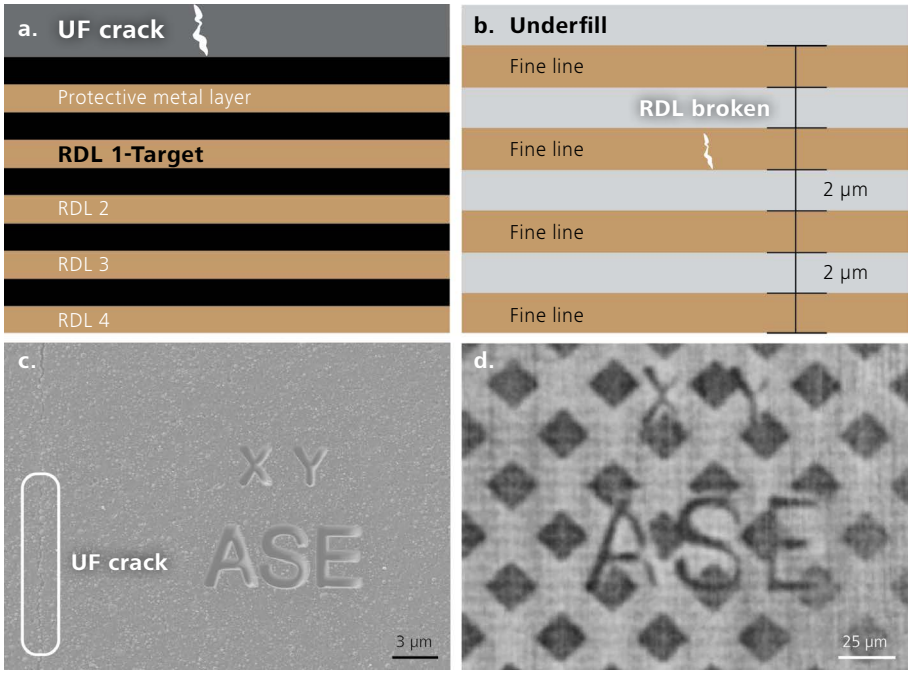

Figure 3 *The case study of FOWLP RDL: a) the schematics of the package structures shows underfill cracks. b) the cross-section shows the RDL broken metal line. c) SEM image shows the FIB-cut fiducial marks "XY" and "ASE" and underfill cracks. d) 3D reconstructed slice of the X-ray scan (3.6 hour) shows the alignment features.*

The 3.6 hour and 0.9 hour scan results were reconstructed by both standard FDK and DeepRecon reconstruction methods, respectively for a comparative study. Figure 4b is an example reconstructed slice with 0.9 hour scan, showing comparable image quality on the fiducial mark to the 3.6 hour scan reconstructed by the standard FDK method (Figure 4a). In both cases, it is clearly visualized of the FIB-cut symbols "XY" and "ASE" created for alignment purpose. This case demonstrated that the new deep-learning based reconstruction method was effective to reduce the scan time by a factor of four, compared with the standard FDK reconstruction.

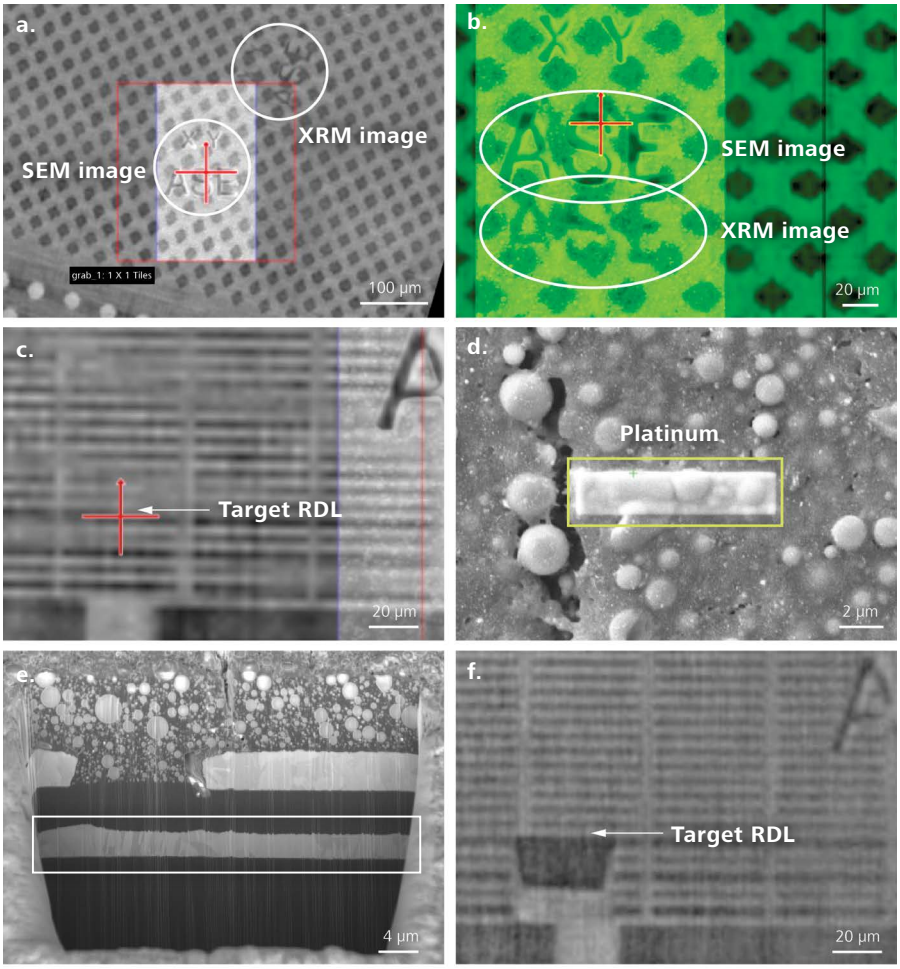

Figure 5 *The workflow detail of the case study of FOWLP RDL. a-b) the alignment of XRM image with SEM image. FIB cut geometric features of "XY" and "ASE" used as fiducial marks for registration. c) 3D reconstructed slice shows the target RDL. d) Platinum bar deposition. e) FIB cut and SEM image of the abnormal RDL. f) 3D X-ray scan validated the target RDL after cross-sectioning.*

Figure 5 is the workflow detail on the FOWLP RDL case study. Figure 5a-b shows that the images of SEM and X-ray scans were overlaid with one on the top of the other, by necessary coordinates translation. As a result, the SEM sample stage was moved to the target RDL (Figure 5c). After Pt deposition (Figure 5d) for tilt angle detection, a FIB cut performed, revealing the abnormal RDL in the green box (Figure 5e). Another 0.9 hour X-ray scan with deep learning reconstruction was followed to verify that the targe RDL was actually processed with FIB-SEM (Figure 5f).

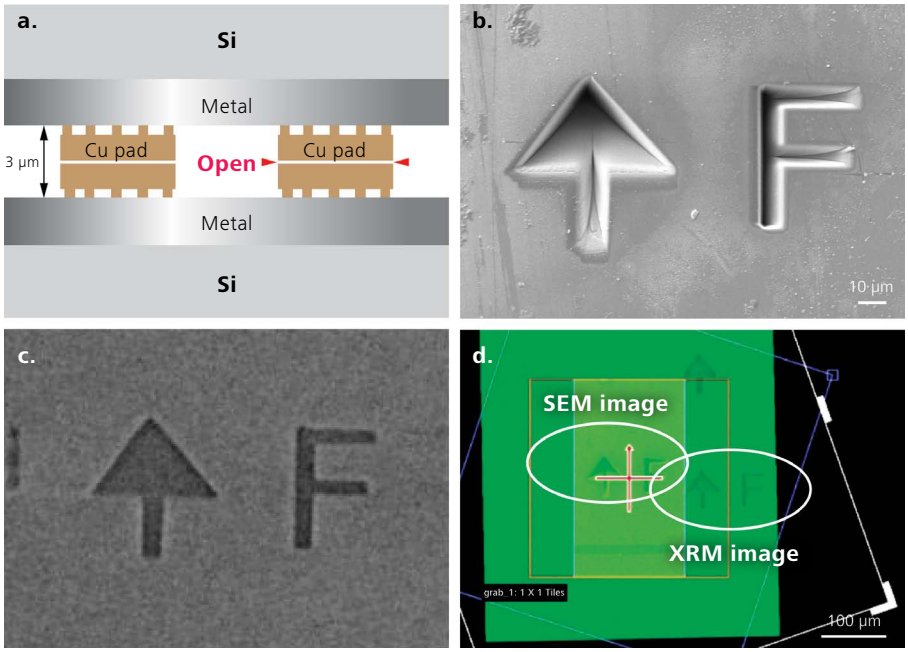

Figure 6 *The case study of hybrid bonds. a) the schematics of the Cu-to-Cu with possible opens. b) SEM image of the FIB cut fiducial marks on surface. c) X-ray image shows the same fiducial marks. d) overlay two images together.*

Hybrid Bonds

Hybrid bonding in heterogenous integration and other advanced IC packages enables sub 10 µm pitch interconnection with high-density external I/Os. However, there are several challenges in processing and failure analysis, such as surface quality, bonding reliability, and Cu-to-Cu misalignment.

Figure 6a shows the diagram of hybrid bonds (3x3 µm) with possible electrical open failure. The fiducial marks with the arrow and letter "F" were milled by FIB with 30 kV and 30 nA shown in Figure 6b. It took about 7 mins for each mark. A 3D X-ray scan at 0.5 µm/pixel resolution for 9 hour was followed (Figure 6c). Figure 6d shows that the images from SEM and X-ray tomography were overlaid each other by necessary translations of the coordinates. Figure 7 shows a comparative study between these two reconstruction methods used in the hybrid bond package case. The 9 hour and 2.25 hour scan results at 0.5 µm/vox were reconstructed by FDK and deep-learning reconstruction methods respectively.

The virtual cross-sectional slice from FDK 9 hour (Figure 7a) and the deep-learning 2.25 hour (Figure 7b) scans resulted in very comparable image quality, clearly visualizing the FIB-processed alignment marks.

Figure 8 is the workflow detail of the hybrid bond case study. Once the images were aligned properly, the SEM sample stage was automatically moved to the target hybrid bond with ease translation (Figure 8a). Following the Pt deposition (Figure 8b), a FIB cut was performed, revealing the opening failure on these two Cu-to-Cu bonds (Figure 8c). Figure 9 shows the further magnified view on the hybrid bond cracks on the right. Another 3D X-ray scan was followed (Figure 8d), having validated that the cut hybrid bonds were indeed the bonds of interest. From electrical testing to the physical failure analysis using the proposed workflow, we concluded that the insufficient wafer planarization was the root cause of bonding failure.

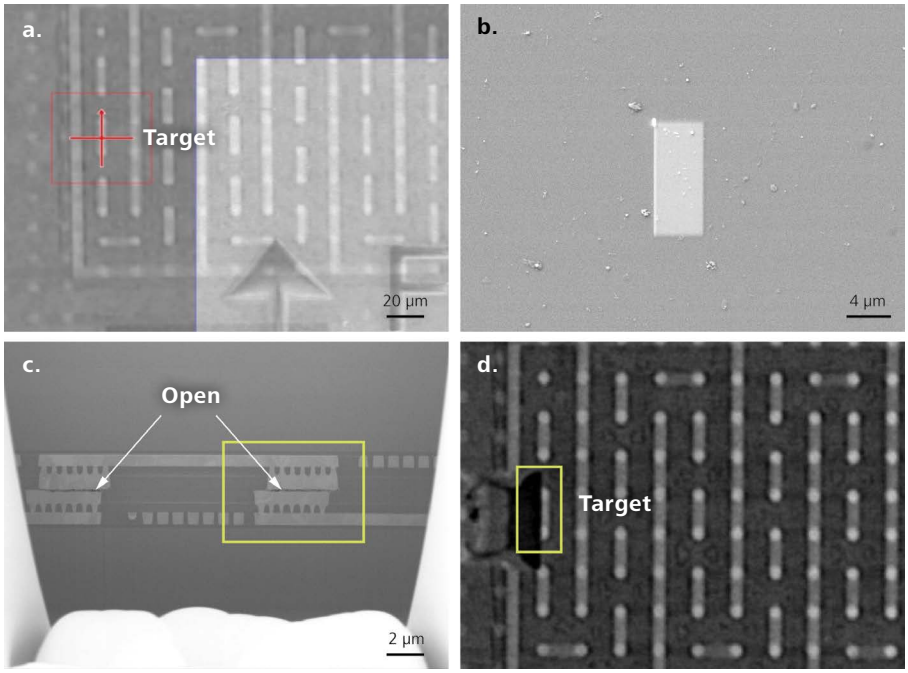

Figure 8 *The workflow detail of the hybrid bond case study. a) move the SEM sample stage to the target hybrid bond. b) SEM Pt deposition. c) the SEM micrograph shows the opening defect between the Cu bonds on the target interconnectors. d) X-ray image validated that the target hybrid bond was FIB cross-sectioned.*

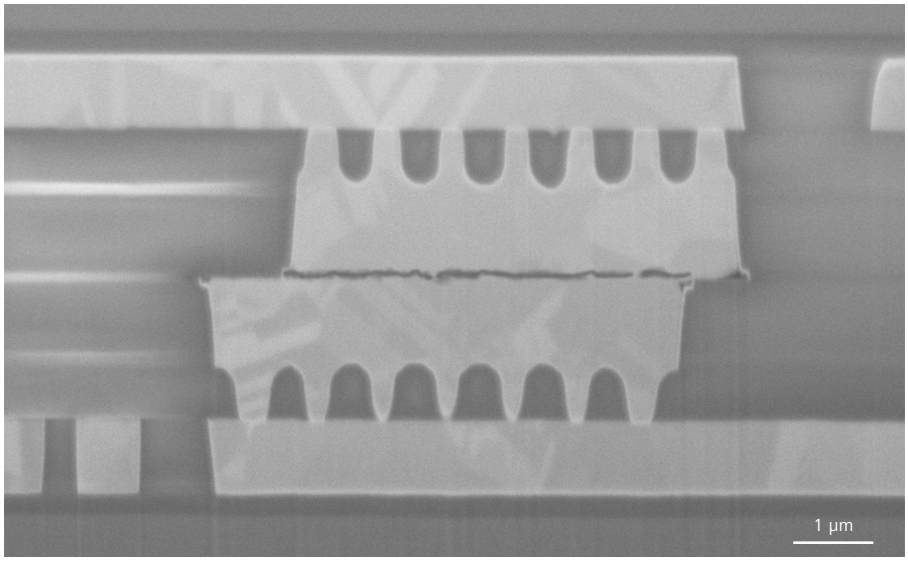

Figure 9 *SEM image shows the further magnified view on the hybrid bond cracks. The zooming-in area is the green box on Figure 8.*

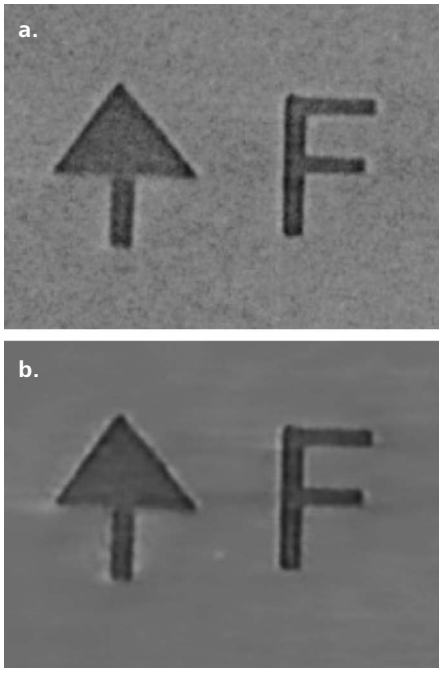

Figure 7 *A comparison of the standard FDK with the deep learning-based reconstruction method. a) the virtual slice shows the fiducial mark acquired by FDK for 9 hour. b) the same slice acquired for 2.25 hour and reconstructed with the deep learning reconstruction.*

Conclusion

We demonstrated a correlative microscopic method and workflow that combine XRM's non-destructive 3D imaging with FIB-SEM cross-sectioning and imaging capabilities, enabling analysts to precisely locate and prepare defects of interest for nanoscale analyses with FE-SEM. AI-powered reconstruction for 3D data acquisition has shown powerful to significantly reduce the time-to-results of the entire workflow. Three use cases were studied for the failure analysis of fine-pitch interconnects in next-generation IC packages. As new package architectures are trending towards 3D packaging and heterogenous integration, the reported workflow can be used for more effective and efficient root cause determination.

References

[1] L. Mirkarimi, A. Gu, L. Hunter, G. Guevara, M. Huynh, R. Katkar, "X-ray Microscopy and Root Cause Analysis in Electronic Packaging", *Proc 41st Int'l Symp for Testing and Failure Analysis,* Portland, OR, Nov. 2015, pp. 430-435. doi: 10.31399/asm.cp.istfa2015p0430

[2] A. Gu, J. Auyoong, "3D Measurement Workflow for Packaging Development and Production Control Using High-Resolution 3D X-ray Microscope", *2018 IEEE 20th Electronics Packaging Tech Confer (EPTC),* Singapore, Dec. 2018. doi:10.1109/EPTC.2018.8654390

[3] S. M. Zulkifli, B. Zee, W. Qiu, A. Gu, "High-Res 3D X-ray Microscopy for Non-Destructive Failure Analysis of Chip-to-Chip Micro-bump Interconnects in Stacked Die Packages", *IEEE 24th Int'l Symp on the Physical and Failure Analysis of Integrated Circuits (IPFA),* Chengdu, China, Jul. 2017. doi:10.1109/IPFA.2017.8060111

[4] S. Li, J. Frame, E. M. Berry, J. Hulog, M. Zhang; A. Gu, M. Terada, D. Taraci, "Detecting Wafer Level Cu Pillar Defects Using Advanced 3D X-ray Microscopy (XRM) with Submicron Resolution", Int'l Symp. for Testing and Failure Analysis, istfa2023p0432, pp. 432-435; https://doi.org/10.31399/asm.cp.istfa2023p0432

[5] A. Gu, A. Andreyev, M. Terada, B. Zee, S. M. Zulkifli, Y. Yang, "Accelerate Your 3D X-ray Failure Analysis by Deep Learning High Resolution Reconstruction Paper," Int'l Symp for Testing and Failure Analysis, No: istfa2021p0291, pp. 291-295, Phoenix, AZ, Dec 2021.

[6] S. M. Zulkifli, B. Zee, Q. Wen, M. Ong; A. Gu, A. Andreyev, M. Terada, Y. Yang, "An Artificial Intelligence Powered Resolution Recovery Technique and Workflow to Accelerate Package Level Failure Analysis with 3D X-ray Microscopy", Int'l Symp for Testing and Failure Analysis, istfa2023p0443, pp. 443-447; https://doi.org/10.31399/asm.cp.istfa2023p0443

[7] A. Gu, M. Terada, H. Stegmann, T. Rodgers, C. Fu and Y. Yang, "From System to Package to Interconnect: An Artificial Intelligence Powered 3D X-ray Imaging Solution for Semiconductor Package Structural Analysis and Correlative Microscopic Failure Analysis," IPFA 2022, Singapore

[8] T. Rodgers; A. Gu; G. Johnson; M. Terada; N. Cohan; V. Viswanathan; M. W. Phaneuf; J. D. Fourestier; E. Ruttan; S. McCracken; S. Costello; A. M Robinson; A. Gibson; A. Balfour, "A Correlative Microscopic Workflow For Nanoscale Failure Analysis and Characterization of Advanced Electronics Packages," Int'l Symp for Testing and Failure Analysis, istfa2022p0319, pp. 319-323; 5 pages https://doi.org/10.31399/asm.cp.istfa2022p0319

Originally Published at ISTFA 2021: Proceedings from the 47th International Symposium for Testing and Failure Analysis Conference

ZEISS

Seeing beyond

Accelerate Your 3D X-ray Failure Analysis by Deep Learning High Resolution Reconstruction

Allen Gu, Andriy Andreyev, Masako Terada
Carl Zeiss Research Microscopy Solutions, 5300 Central Parkway, Dublin, CA 94568, USA
Bernice Zee, Syahirah Mohammad-Zulkifli
Advanced Micro Devices (Singapore) Pte Ltd, Device Analysis Lab 508 Chai Chee Lane, Singapore 469032
Yanjing Yang
Carl Zeiss X-ray Microscopy Applications, 50 Kaki Bukit Place, Singapore 415926

Abstract

Over the past decade, 3D X-ray has played a critical role in semiconductor package failure analysis (FA), primarily owing to its non-destructive nature and high resolution capability [1,2]. As novel complex IC packages soar in recent years [3,4], X-ray failure analysis faces increasing challenges in imaging new advanced packages because IC interconnects are more densely packed in larger platforms. It takes several hours to overnight to image fault regions at high resolution or crucial details of a defect remain undetected. A high-productivity X-ray solution is required to substantially speed up data acquisition while maintaining image quality. In this paper, we propose a new deep learning high-resolution reconstruction (DLHRR) method, capable of speeding up data acquisition by at least a factor of four through the implementation of pre-trained neural networks. We will demonstrate that DLHRR extracts signals from low-dose data more efficiently than the conventional Feldkamp-Davis-Kress (FDK) method, which is sensitive to noise and prone to the aliasing image artifacts. Several semiconductor packages and a commercial smartwatch battery module will be analyzed using the proposed technique. Up to 10x scan throughput improvement was demonstrated on a commercial IC package. Without the need of any additional X-ray beam-line hardware, the proposed method can provide a viable and affordable solution to turbocharge X-ray failure analysis.

Introduction

As the era of transistor scaling driven technology is coming to an end in the semiconductor industry, packaging innovation strives to continuously improve the performance and reliability of electronics products. The trend of 3D packaging and heterogenous integration has presented increasing challenges to existing FA techniques because of more complex multichip architectures and more miniaturized interconnects. The 3D X-ray workflow is known for enhancing FA success rates by its non-destructive and high-resolution imaging capabilities. However, its applications to advanced packages have become less effective due to increasing package complexity and density, together with the surging demand for non-destructive X-ray inspection. A faster X-ray solution is required to substantially enhance the imaging efficiency so that the user does not have to compromise image quality and scan throughput in high resolution imaging.

Computed tomography (CT) image reconstruction, a necessary step in any 3D X-ray workflow, converts 2D projection images to a 3D volume. Most commercial CT systems utilize the traditional FDK algorithm for reconstruction. It can generate good quality images in a fast and reliable reconstruction process. In addition, it does not require as high computing power as other reconstruction methods such as iterative reconstruction. The FDK method, however, is sensitive to photon starvation and resulting images are prone to a variety of under-sampling artifacts. Consequently, a high number of projections, and/or long exposure time per projection are required for reducing image noise and artifacts. Long scans are necessary for high quality data acquisition. In this work, we will introduce and evaluate a new deep learning-based reconstruction method to overcome this hurdle.

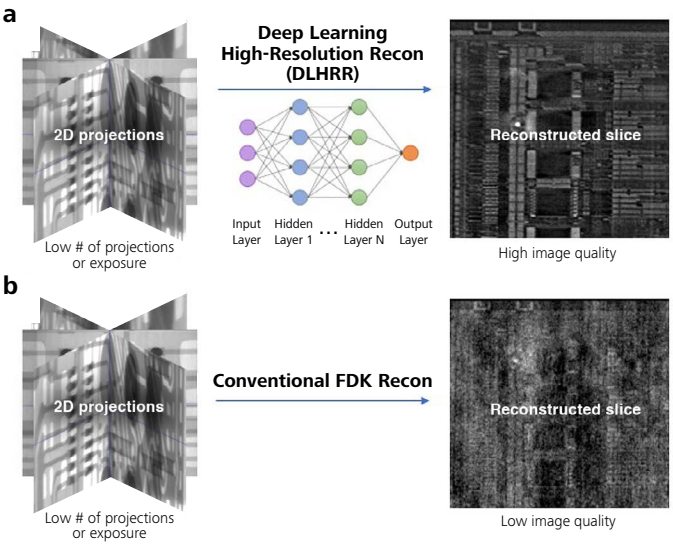

Figure 1 Schematics of the architecture of the proposed DLHRR method a) and its performance advantage over the conventional FDK method b). With the same low number of projections, DLHRR generates higher quality images than the conventional FDK method.

Deep Learning High-resolution Reconstruction

Deep learning based convolutional neural networks have shown excellent performance in numerous computer vision tasks such as recognition, segmentation, resolution improvement, and denoising [5-8]. However, the reported methods are not directly useful to X-ray microscopy, where an actual 3D image has to be reconstructed from a set of 2D X-ray projections, in which the corrections for source spectrum, photon statistics, sample drifts and X-ray scattering are required to maintain the highest image resolution and quality.

The new convolutional neural network method is based on the "noise2noise" model and approach [9] with the ZEISS proprietary cost function and training data preparation protocol available under ZEISS DeepRecon Pro. The network proposed and evaluated in this work (Fig. 1) is more suitable for high-resolution image reconstruction, because it addresses image quality degradation in the scenario of low pixel counts or insufficient number of projections [10]. The training input is a set of low number of projections with high-noise pixels, and the training target is an image created from a high number of projections with low-noise pixels, which serves as the "ground truth" data.

The training of the network is done in a manner that it is applicable to the desired X-ray microscope data acquisition settings and a given sample class. The model will need to be retrained if such parameters change. However, the network is quite lightweight and can be re-trained within 3 hours on a relatively mid-range professional workstation (Dell Precision 7920) utilizing two professional GPUs totaling 48 GB of video RAM. Once the network is trained, it can be applied to all the tomographic data that belongs to the same class and the reconstruction itself takes less than 5 minutes for a 1000^3 voxels image volume. We intentionally minimized the number of parameters to be optimized to just one that controls the noise level dictated by the desired total acquisition scan time. It works especially well when the imaging task consists of several samples or ROIs that need to be imaged in the same or similar manner, since every subsequent sample/ROI does not require retraining of the network. Given the simplicity of the training process and the comparatively short training duration that is of the same order of magnitude as iterative reconstruction, we foresee that DLHRR will be used on unique samples as well.

Since the applicability of the network is narrowed to a strict sample class and acquisition conditions, the network can be trained on as little as one tomography. There are also no strict requirements towards the training data, other than the sample needing to be well represented with all characteristic features in the field-of-view. It is worth noting that even a single tomographic acquisition is three dimensional in nature, containing hundreds or thousands of 2D images. This provides the network with enough training data. Furthermore, the training data are augmented during the training process to account for potential variations in sample and data acquisition conditions. Overall, the images reconstructed by the DLHRR method routinely result in better quality than the FDK-reconstructed images, in which the critical structural information is frequently lost due to the under-sampling noise and artifacts.

Results

In our first case study, 3D X-ray data was acquired at 0.7 µm/vox resolution on a 50x50 mm AMD HBM-µbump 2.5D package (Fig. 2a). The fault region was µbump joint cracks at the high-bandwidth memory stack and interposer interface, as shown in Fig. 2b. It is a 3D color-rendering image. With a typical setting of FDK reconstruction, 1,600 projections were acquired in a 9.6 hour tomography, revealing ~ 1 µm thick bump cracks (Fig. 2c-d). The DLHRR slices in Fig. 2e-f) showed very similar image quality on the corresponding cracks with only 400 projections for a 2.4 hour scan. This case demonstrated that DLHRR successfully learned to differentiate signal and noise from the training data, achieving equivalent image quality without losing the visibility of the small features in a scan 4x faster than FDK.

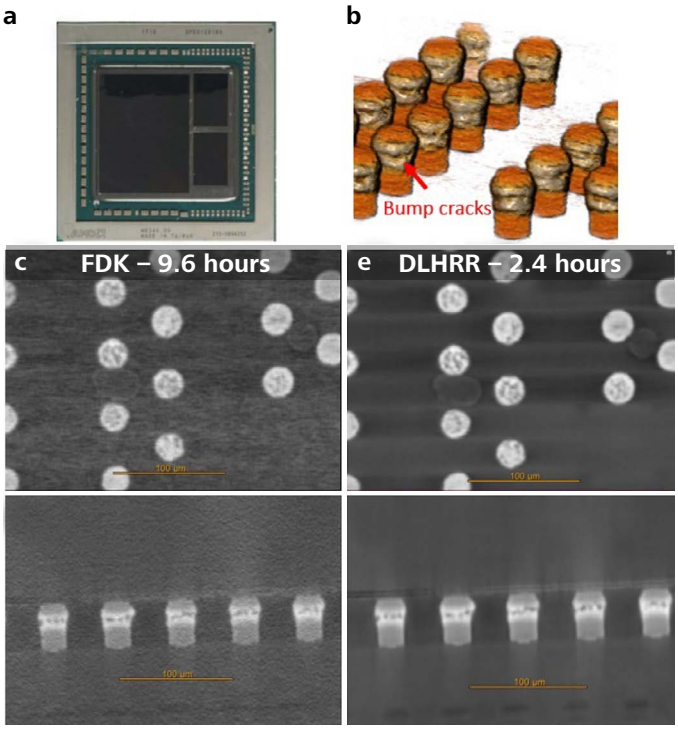

Figure 2 *Comparison of the DLHRR results to FDK on a 50x50 mm AMD HBM-µbump package. a) sample, b) a 3D color-rendering image at 0.72 µm/vox resolution, c-d) virtual cross-section slices from the FDK 9.6 hour scan, e-f) virtual slices from the DLHRR 2.4 hour scan. c) and e) are the top-down views, and d) and f) are the cross-sectional views.*

In the second case study, X-ray scans were obtained at 1.5 µm/vox resolution on a commercial 10x10 mm smartphone A8 package. Both FDK and DLHRR reconstruction methods were performed for comparison. Since there were no known electrical open or short failures in the test sample, we focused on solder ball and via voids, a common defect in IC packages. Fig. 3a) shows an example slice from the 6 hour scan reconstructed by FDK. The image quality is acceptable with this long scan. As the X-ray dose decreased by a factor of ten, the traditional FDK method showed its inefficiency to extract signal from the 0.6 hour scan (data not shown). By contrast, the slice from the same short scan but reconstructed by DLHRR maintained the high image quality – no image detail was lost (Fig. 3b).

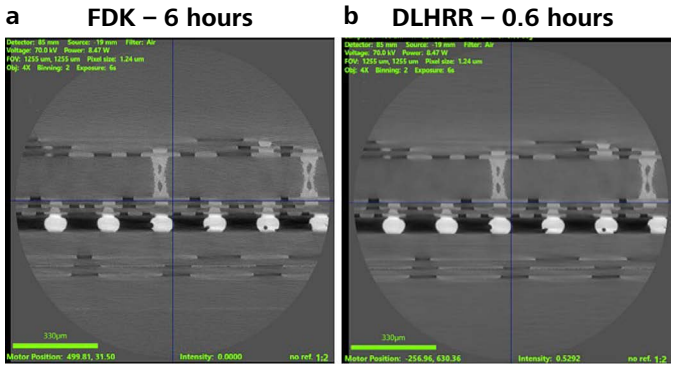

Figure 3 *A comparison of the virtual slices extracted from a) the FDK 6 hour scan, b) the DLHRR 0.6 hour scan at 1.5 µm/voxel resolution on a smartphone A8 package.*

Analysis time is critical in semiconductor package reliability testing because package structures may alter over the test cycles. To understand throughput improvement for 3D X-ray application in reliability testing, we acquired data on a 2.5D interposer package tested by using the JEDEC thermal cycle standard (Fig. 4a). The 4 hour and 1 hour scan results at 0.7 µm/vox were reconstructed by both DLHRR and FDK methods for comparison. Fig.4b is the 3D color-rendering image from the FDK 4 hour scan, showing the defective bumps at the corner of the package. The virtual cross-sectional slice from FDK 4 hour (Fig. 4c) and DLHRR 1 hour (Fig. 4d) scans resulted in very comparable image quality, clearly visualizing ~ 2 µm cracks at C4 bumps, the byproduct of the thermal cycle. With the high-level noise in the FDK 1 hour data (not shown), the crack information may be misinterpreted. This case demonstrated that the DLHRR method was effective to reduce the scan time by a factor of four, compared with the standard FKD reconstruction.

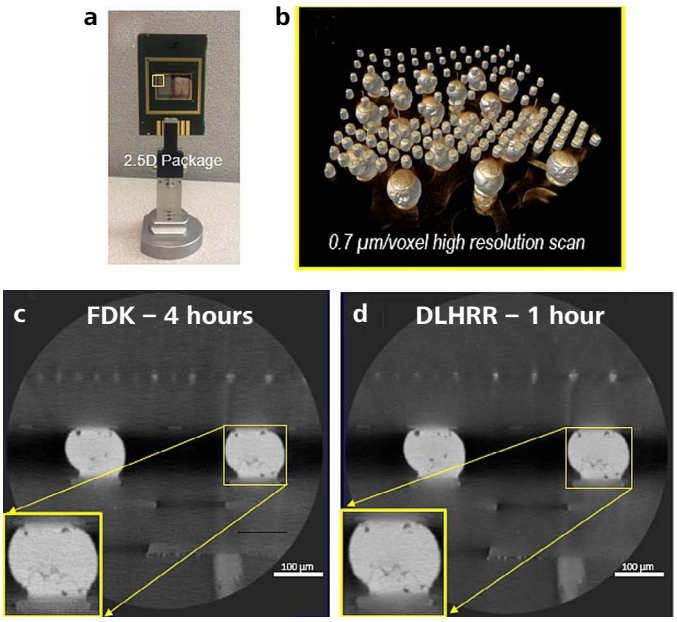

Figure 4 *DLHRR results used in the reliability study of a 50x75 mm 2.5D interposer package. a) sample, b) a 3D color-rendering image for the defective corner of the package, acquired at 0.7 µm/vox, c) a reconstructed slice by the FDK 4 hour scan, d) a reconstructed slice by the DLHRR 1 hour scan. The insets in c-d) are the digitally zoomed-in images on the cracked bump.*

3D X-ray imaging and analysis are important in quality inspection and longevity study of lithium-ion batteries. A high-resolution interior tomography on a battery sample can take ~24 hours with the traditional FDK reconstruction. To test the scan throughput improvement by the new DLHRR method, we acquired 3D X-ray data on a commercial smartwatch battery module, which were later reconstructed by these two methods for a comparative study (Fig. 5). The baseline data from the FDK 24 hour scan are shown in Fig. 5a-b). When reducing the number of projections by a factor of four (Fig. 5c), the FDK slice showed a high level of noise, which shadowed the visibility of the polymer separator, a key structure relevant to battery performance. The low data quality resulted from under-sampling noise and artifacts in the FDK reconstruction, which would make it difficult for subsequent segmentation and quantification. By contrast, the DLHRR slice (Fig. 5d) showed clear particle boundary definitions even at the reduced scan time at 6 hours. It was found that the contrast-to-noise ratio from the DLHRR 6 hour scan is even higher than the FDK 24 hour scan. This case further demonstrated the effectiveness of the new DLHRR reconstruction method to reduce the data acquisition time by a factor of four.

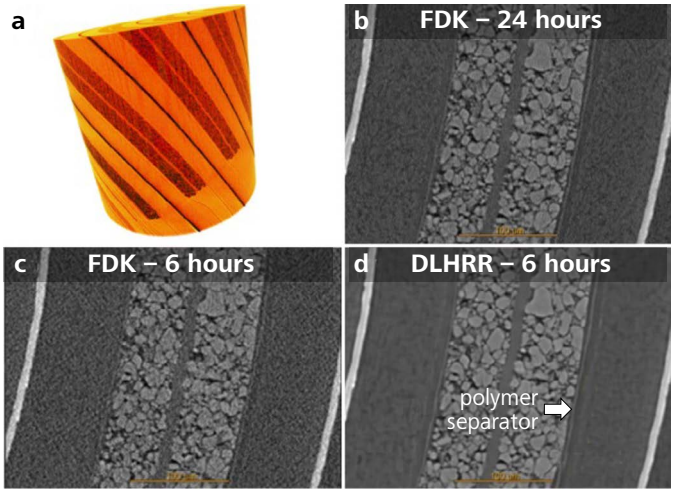

Figure 5 *A comparative study of the DLHRR results to FDK on a commercial smartwatch battery module. The tomography was acquired at 0.53 µm/vox resolution. a) a 3D color-rendering image from the FKDK 24 hour scan, b) a virtual slice from the FKD 24 hour scan, c) a virtual slice from the FDK 6 hour scan, d) a virtual slice from the DLHRR 6 hour scan.*

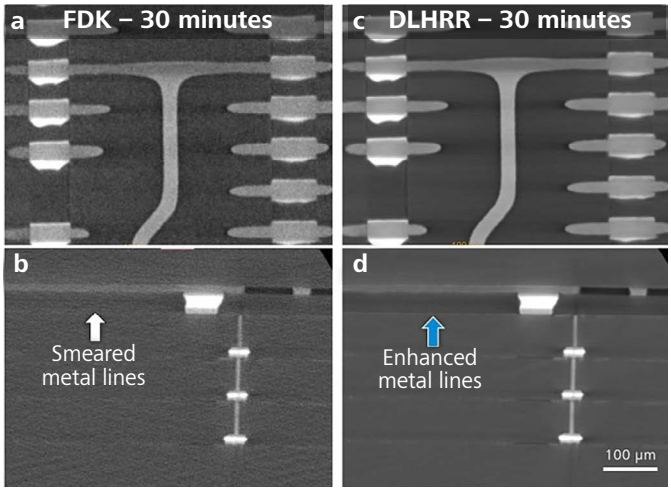

Figure 6 *With the same scan time, the DLHRR results in c-d) show superior image quality over the FDK results in a-b). The data was acquired on a commercial µbump-TSV DRAM sample at 1 µm/vox resolution. The blue arrow in d) shows an enhanced contrast-to-noise ratio on the metal lines, which were smeared in the FDK result. a) and c) are top-down views. b) and d) are cross-sectional views.*

So far we have demonstrated that the DLHRR method can be used for reducing scan time significantly on several cases. It can also be used for improving image quality in a same scan time setting. 3D X-ray data were acquired at 1 µm/vox resolution on a commercial 4-High DRAM package (Fig. 6). The sample was chosen because it has about 2 µm thin metal lines on the top of dies, a good target for image quality assessment. With FDK reconstruction, 400 projections were acquired in a 30 minute tomography. The resulting top-down view and cross-sectional views are showed in Fig. 6 a-b. The metal lines however were largely smeared due to the high level of noise generated by the traditional reconstruction method in the low X-ray dose tomographic scan (Fig. 6b). The small structure may be overlooked due to the low image quality. Longer scans are generally required to retain this small feature. With the DLHRR method, the visibility of the same metal lines was largely enhanced (Fig. 6d) even in the short scan data. During the network training process, the machine has learned to recognize the small feature and the surrounding noise. Compared with the high level of noise in Fig. 6a, the DLHRR results show higher contrast-to-noise ratio in the top-down view (Fig. 6c). This case demonstrated the effectiveness of the new DLHRR reconstruction method to improve image quality in the same scan time, especially for short scans. As modern advanced packages become more complex, defects and failures are more difficult to image and characterize. Highest image quality with shortest scan time is always preferred in 3D X-ray failure analysis workflows to enhance the success rate of root cause analyses.

3D volume stitching plays an important role in FA fault isolation, intellectual property intelligence and reverse engineering applications. The benefit is to achieve higher resolution for a field of view (FOV) through multiple-volume stitching, overcoming the detector size limitation. However, the total scan time is long because of the multi-volume data acquisition. The DLHRR method can elevate the scan efficiency without losing image quality because the time reduction for a single volume scan can be applied to other volumes without the need of an additional network training. The test sample was the entire accelerator/gyroscope package, as indicated by the red box in Fig. 7a, of a commercial smartphone mother board. We acquired 3x3 volumes with 1.6 µm/voxel resolution for each volume. With a typical FDK reconstruction setting, it took 100 minutes for each volume. The nine volumes took the total of 900 minutes and the stitched data are shown in Fig. 7 b-c. With the DLHRR reconstruction method, only 25 minutes per scan was required. As shown in Fig. 7e, the 25 minutes scan and DLHRR reconstruction generated excellent image quality. By contrast, the result from a 25 minutes scan and FDK reconstruction showed a high level of noise and rich streak artifacts (Fig. 7d), which may cause a failure of stitching. The visibility of the Si structure was overshadowed by the noise. In this case, the DLHRR method succeeded to reduce the total scan time to 225 minutes in the data acquisition of all the stitched volumes, which requires 900 minutes scan with the traditional FDK method. The trained network model based on the center volume was successfully applied on all other volumes. We demonstrated that the DLHRR can be used to improve the image resolution over larger FOVs through more efficient multiple-volume data acquisition and stitching.

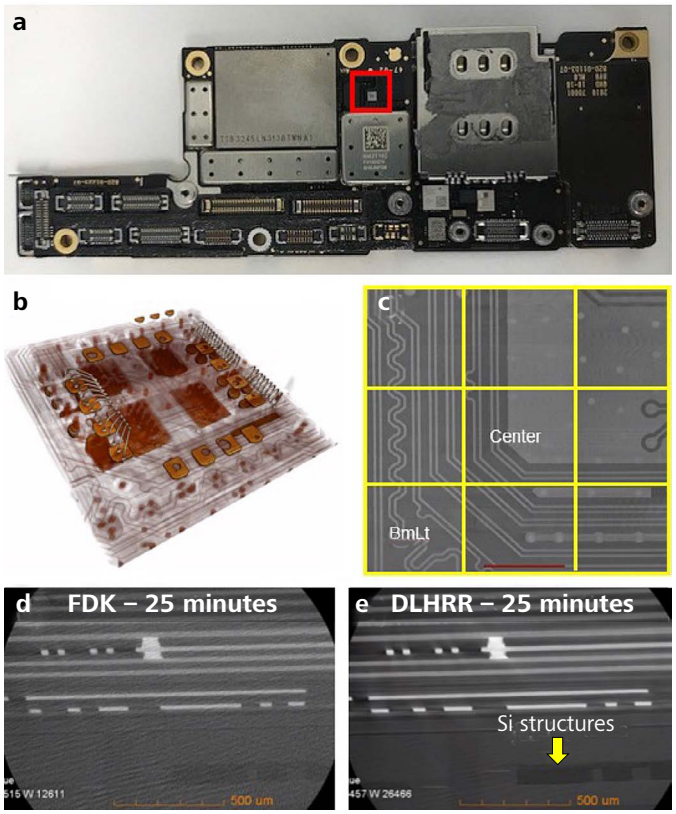

Figure 7 *DLHRR was used in a test of multiple volumes stitching. a) an accelerator/ gyroscope package in a commercial smartphone motherboard. b) 3x3 stitched volumes. c) a virtual cross-section of the stitched volume from the FDK reconstruction. d) a virtual slice from the FDK 25 minute scan. e) a corresponding slice from the DLHRR 25 minute scan. Both scans were acquired at 1.6 µm/voxel resolution.*

Conclusion

The impacts of artificial intelligence technology have been seen across most industrial segments and commercial services such as transportation, healthcare, education, on-line shopping, finance and many more. This technological development provides a golden opportunity for the electronics failure analysis society to enable capability improvement and revolution. In this report, we demonstrated a deep learning based high-resolution reconstruction technique which can be used to substantially shorten X-ray failure analysis workflows. The throughput improvement by a factor of four or ten was demonstrated for several semiconductor package examples. Since the network can be trained on as little as one tomography dataset, its application range is limited to the sample class and acquisition condition specified by that training dataset. Network applicability to broad sample classes can be improved with further development. It is also possible to extend 3D X-ray applications to other high-productivity areas such as fault screening and isolation, package construction analysis, and even in-line inspection and metrology.

Acknowledgements

We thank Dr. Lars Omlor, Dr. Matthew Andrew, and Dr. Christoph Hilmar Graf vom Hagen, Carl Zeiss X-ray Microscopy, Dublin, CA, USA, for the DLHRR algorithm development, and instrumental discussions on its applications.

Reference

[1] L. Mirkarimi, A. Gu, L. Hunter, G. Guevara, M. Huynh, R. Katkar, "X-ray Microscopy and Root Cause Analysis in Electronic Packaging", Proc 41st Int'l Symp for Testing and Failure Analysis, Portland, OR, Nov. 2015, pp. 430-435. doi: 10.31399/asm.cp.istfa2015p0430

[2] S. M. Zulkifli, B. Zee, W. Qiu, A. Gu, "High-Res 3D X-ray Microscopy for Non-Destructive Failure Analysis of Chip-to-Chip Micro-bump Interconnects in Stacked Die Packages", IEEE 24th Int'l Symp on the Physical and Failure Analysis of Integrated Circuits (IPFA), Chengdu, China, Jul. 2017. doi:10.1109/IPFA.2017.8060111

[3] T. Gregorich, M. Terada, C. Hartfield, A. Gu and J. Vardaman, "Non-destructive Characterization of Application Processor Panel Level Package Used in Galaxy Smartwatch", 2019 Int'l Wafer Level Packaging Confer., San Jose, CA, Oct. 2019, pp. 1-7. doi: 10.23919/IWLPC.2019.8914126

[4] A. Gu, J. Auyoong, "3D Measurement Workflow for Packaging Development and Production Control Using High-Resolution 3D X-ray Microscope", 2018 IEEE 20th Electronics Packaging Tech Confer (EPTC), Singapore, Dec. 2018. doi:10.1109/EPTC.2018.8654390

[5] K. Simonyan and A. Zisserman, "Very Deep Convolutional Networks for Large-Scale Image Recognition", Int'l Confer. on Learning Representations, 2015, arXiv:1409.1556

[6] V. Badrinarayanan, A. Kendall and R. Cipolla, "SegNet: A Deep Convolutional Encoder-Decoder Architecture for Image Segmentation", IEEE Transactions on Pattern Analysis and Machine Intelligence, vol. 39, issue 12, 2017

[7] C. Ledig, L. Theis, F. Huszar, J. Caballero, A. Cunningham, A. Acosta, A. Aitken, A. Tejani, J. Totz, Z. Wang and W, Shi, "Photo-Realistic Single Image Super-resolution Using a Generative Adversarial Network" in Computer Vision and Pattern Recognition, 2017

[8] K. Zhang, W. Zuo, Y. Chen, D. Meng and L. Zhang, "Beyond a Gaussian Denoiser: Residual Learning of Deep CNN for Image Denoising", IEEE Transactions on Image Processing, vol. 26, issue, 7, 2017

[9] J. Lehtinen, J. Munkberg, J. Hasselgren, S. Laine, T. Karras, M. Aittala, and T. Aila, "Noise2Noise: Learning Image Restoration without Clean Data," 35th Int. Conf. Mach. Learn. ICML 2018 7 (2018).

[10] M. Andrew, R. Sanapala, A. Andreyev, H. Bale, C. Hartfield, "Supercharging X-ray Microscopy Using Advanced Algorithms", Microscopy and Analysis, pp17, Nov/Dec 2020

Follow us on social media:

microscopy@zeiss.com
www.zeiss.com/semiconductor-microscopy